Relay-Aided Multi-user OFDM Relying on Joint Wireless Power Transfer and Self-Interference Recycling

A. A. Nasir[1], H. D. Tuan[2], E. Dutkiewicz[2], H. V. Poor[3], and L. Hanzo[4]

Abstract—**Relay-aided multi-user OFDM is investigated under which multiple sources transmit their signals to a multi-antenna relay during the first relaying stage and then the relay amplifies and forwards the composite signal to all destinations during the second stage. The signal transmission of both stages experience frequency selectivity. The relay is powered both by an energy source through the wireless power transfer as well as by the energy recycled from its own self-interference during the second stage. Accordingly, we jointly design the power allocations both at the multiple source nodes and at a common relay node for maximizing the network's sum-throughput, which poses a large-scale nonconvex problem, regardless whether proper Gaussian signaling (PGS) or improper Gaussian signaling (IGS) is used for signal transmission to the relay. We develop new alternating descent procedures for solving our joint optimization problems, which are based on closed-forms and thus are of very low computational complexity even for large numbers of subcarriers. The results show the superiority of IGS over PGS in terms of both its sum-rate and individual user-rate. Another benefit of IGS over PGS is that the former promises fairer rate distribution across the subcarriers. Moreover, the recycled self-interference also provides a beneficial complementary energy source.**

Index Terms—**Full-duplexing for transmitting information and recycling energy, multi-user OFDM, large-scale nonconvex optimization, online computation.**

I. INTRODUCTION

Short-range wireless power transfer is potentially capable of powering the Internet of Things (IoTs) [1]. Indeed, the integration of wireless information and power transfers has emerged as a promising solution for eco-friendly, always-on, wireless communications [2]. Explicitly, for convenient simultaneous wireless information and power transfer (SWIPT), the received signal conveying both information and energy has to be split either by power-splitting or time-switching [3]. Our recent studies [4]–[6] have shown that SWIPT is outperformed by

[1]Department of Electrical Engineering and Center for Communication Systems and Sensing at King Fahd University of Petroleum & Minerals (KFUPM), Dhahran 31261, Saudi Arabia (e-mail: anasir@kfupm.edu.sa); [2]School of Electrical and Data Engineering, University of Technology Sydney, Broadway, NSW 2007, Australia (email:Tuan.Hoang@uts.edu.au, Eryk.Dutkiewicz@uts.edu.au); [3]Department of Electrical Engineering, Princeton University, Princeton, NJ 08544, USA (email: poor@princeton.edu); [4]School of Electronics and Computer Science, University of Southampton, Southampton, SO17 1BJ, U.K. (e-mail: lh@ecs.soton.ac.uk)

time-fraction based separate information and energy transfers, where a fraction of the time-slot is used for information transfer and the remaining fraction for energy transfer. More explicitly, the latter has the edge in terms of performance, design freedom, practical implementation and computational tractability of its signaling design.

Full-duplex (FD) techniques relying on 'almost' co-located transmit and receive antennas operating within the same time- and frequency-band have been proposed for simultaneous signal transmission and reception (STR) [7], [8]. However, the self-interference leaked from the high-power transmit signals to the low-power received signals cannot be sufficiently mitigated at the current sate-of-the-art, even if both analogue- and digital-domain cancellation is combined with physical transmit/receive antenna-separation [9]. Again, time-fraction based separate signal transmission and reception outperforms STR [10], and it is also practical for macro-cell communication [11], which would be unrealistic for STR. However, FD techniques are capable of exploiting the self-interference impinging upon the receiver antennas for beneficially harvesting energy from it [12], [13], hence making it a precious complementary energy resource [14]–[22]. This FD philosophy has been adopted in several recent studies for wirelessly-powered relaying, where an energy-constrained relay node replenishes its battery by harvesting energy both from the energy signal provided by the energy source and from its own self-interference (see e.g. [14], [22]–[27] and references therein).

Orthogonal frequency division multiplexing (OFDM) is the most popular technique of combating frequency selectivity in multipath channels [28]. Here, it is important to mention that whilst information is typically transmitted through frequency selective channels [29], wireless power transfer is only meaningful over strong, non-dispersive, short-range channels [13].

Proper Gaussian signaling (PGS) carries information by circular (proper) Gaussian signals in conventional wireless communication. However, it has been shown that improper Gaussian signaling (IGS) [30], which carries information by noncircular (improper) Gaussian signals, is capable of improving the information throughput of interference-limited networks [31]–[34]. More particularly, IGS has been shown to have a higher max-min throughput than PGS [33]–[36]. However, the performance limits of IGS-based OFDM are still unknown, which requires the solution of large-scale nonconvex problems. Only a few sub-carriers were considered in [37] for avoiding the complexity issues in designing IGS for an OFDM-based cognitive underlay radio system.

Against the above background, this paper considers relay-aided OFDM relying on joint energy transfer and self-

interference recycling. The source and destination nodes are located far apart from each other, hence they communicate via a multi-antenna relay node. There is also a dedicated energy source in the relay's vicinity for transferring energy to it. Information transmission from the sources to the destinations is implemented in two-phases. During the first phase, the sources send their signals to the relay. During the second phase, the relay switches to FD mode: it amplifies and forwards the received signals to all destinations, while its receive antennas harvest energy both from the energy-transfer of the energy source and from its own self-interference. Our objective is to design joint power allocation for the source and relay nodes for maximizing the sum-throughput of the network. The paper goes beyond the recent research contribution of [13], [18]–[21], [27], which did not consider multi-user communication and nor did they investigate IGS in OFDM-based communications. Explicitly, the key contributions of this treatise are as follows:

- This is the first paper to consider IGS in multi-user OFDM communication assisted by a wirelessly powered relay. The sum-throughput maximization problem of the joint power allocation design of multiple sources and a common relay node is quite challenging to solve, even for a conventional PGS based OFDM system. This is because the problem is not only non-convex but it is also of a large-scale nature due to having many subcarriers. The scale of challenge is further escalated for an IGS based OFDM system due to having additional variables.
- As a remedy, we propose novel alternating descent algorithms for solving these problems, which are based on *closed-form* expressions for improving the feasible points. These new low-complexity computational procedures allow us to analyze the performance of both PGS and IGS based OFDM systems having many subcarriers.
- Our extensive simulation results analyze both PGS and IGS based OFDM systems in terms of their sum-rate, individual user-rate, and rate-distribution across the subcarriers. The results show the superiority of IGS over PGS in terms of both its sum-rate and individual user-rate. Another benefit of IGS over PGS is that the former promises fairer rate distribution both across the subcarriers and among the users. Moreover, the results show that the improvement in the sum-rate due to the recycled self-interference is about 0.05 bps/Hz over a wide-range of considered simulation parameters.

Our novel contributions are boldly and explicitly contrasted to the state-of-the-art in Table I at a glance.

The paper is organized as follows. Following the Introduction, Section II describes our system model and problem formulation. The alternating descent algorithms under PGS and IGS are developed in Section III and Section IV, respectively. Section V is devoted to our simulations and Section VI concludes the paper.

Notation. Denote by $\mathcal{C}(0, \chi)$ the set of all circular (proper) Gaussian variables of zero mean and covariance χ. Particularly, $\mathbb{E}(|s|^2) = \chi$ and $\mathbb{E}(s^2) = 0$. A Gaussian variable s is improper whenever $\mathbb{E}(s^2) \neq 0$. $\mathrm{diag}[x_m]_{m=1,\ldots,M}$ is a

TABLE I
RELATED CONTRIBUTIONS.

	this paper	[12]	[13]	[33]–[35]	[37]
OFDM	✓		✓		✓
IGS	✓			✓	✓
Power trans. & recycl.	✓	✓	✓		
MU communciation	✓			✓	

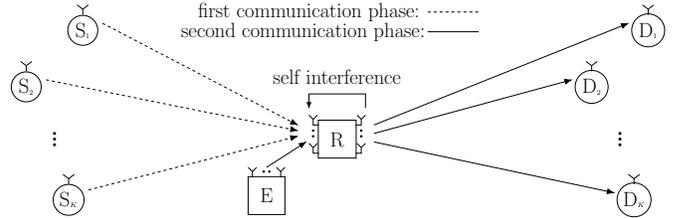

Fig. 1. Wireless-powered relaying with self-energy recycling.

diagonal matrix with x_m, $m = 1, \ldots, M$, on its diagonal. For a matrix X, $X(i, j)$ is its (i, j)-th entry, $[X]^2 = XX^H$, $\langle X \rangle = \mathrm{trace}(X)$, $\mathrm{vec}(X)$ stacks its columns into a single vector, and $X \succeq 0$ means X is a Hermitian symmetric positive definite matrix. For matrices X and Y, $\langle X, Y \rangle$ is their dot product, i.e. $\langle X^H Y \rangle$, and $X \otimes Y$ is their Kronecker product. The following identities can be found in [38]: $\langle X, [HA]^2 \rangle = \langle H^H XH, [A]^2 \rangle$ and $\mathrm{vec}(AXH) = (H^T \otimes A)\mathrm{vec}(X)$ for the matrices X, A and H of appropriate size.

We will use the following inequalities [39]

$$\ln(1 + \frac{|x|^2}{y}) \geq \ln(1 + \frac{|\bar{x}|^2}{\bar{y}}) - \frac{|\bar{x}|^2}{\bar{y}} + 2\frac{\Re\{\bar{x}^* x\}}{\bar{y}}$$
$$- \frac{|\bar{x}|^2}{\bar{y}(\bar{y} + |\bar{x}|^2)}(|x|^2 + y) \quad (1)$$

for all $x \in \mathbb{C}$, $\bar{x} \in \mathbb{C}$, $y > 0$, and $\bar{y} > 0$, and

$$\ln\left|I_2 + [V]^2(Y)^{-1}\right| \geq \ln\left|I_2 + [\bar{V}]^2(\bar{Y})^{-1}\right|$$
$$- \langle(\bar{Y})^{-1}, [\bar{V}]^2\rangle + 2\Re\{\langle(\bar{Y})^{-1}\bar{V}, V\rangle\}$$
$$- \langle(\bar{Y})^{-1} - (\bar{Y} + [\bar{V}]^2)^{-1}, [V]^2 + Y\rangle, \quad (2)$$

for all matrices $V, Y \succ 0$, $\bar{V}$, and $\bar{Y} \succ 0$ of size 2×2. Observe that the right hand side (RHS) of (1) ((2), resp.), which is a concave quadratic function, matches with its right hand side (RHS) at $(\bar{x}, \bar{y})$ (($\bar{V}, \bar{Y}$), resp.). As such the RHS of (1) ((2), resp.) is a tight concave quadratic minorant of its LHS [40].

II. SYSTEM MODEL AND PROBLEM FORMULATION

Fig. 1 illustrates the communication network to be considered in the paper, which consists of a relay supporting the communications in pairs between K source nodes (SNs) and K destination nodes (DNs). Furthermore, there is an energy source in the relay's vicinity to provide a wireless energy supply. There is no direct communication link between the SNs and DNs as they are far apart. The SNs and DNs are equipped with a single antenna, while the relay is equipped with M transmit antennas (TAs) and M receive antennas (RAs). The

energy source is equipped with M_E antennas. The SN to relay node (RN) and RN-DN channels are frequency selective and OFDM is employed for combating the dispersion. However, the channel between the energy source and relay is frequency flat due to the short distance between them (for practical power transfer) . Hence, the energy signal is transmitted by a single carrier. For simplicity, refer to SNs and DNs by S_k and D_k with $k \in \mathcal{K} \triangleq \{1, \ldots, K\}$.

During the first phase, the SNs send their signals to the RN which are amplified and forwarded to all DNs in the second stage. Within this second phase, the energy source sends an energy signal to the RN, which harvests energy both from the received energy signal and also from its own self-interference (SI). Naturally, the energy-constrained RN cannot totally rely on its own SI for replenishing its battery, and thus needs a dedicated energy source in its vicinity [17], [24].

A. Information processing

Assume that the OFDM scheme has N subcarriers, indexed by $n \in \mathcal{N} \triangleq \{0, 1, \ldots, N-1\}$. Denote the transformation matrix of the N-point fast Fourier transform (FFT) by $F_N \in \mathbb{C}^{N \times N}$, whose entries are given by $F_N(n', n) = \frac{1}{\sqrt{N}} e^{j \frac{-2\pi}{N} n' n}$, $(n', n) \in \mathcal{N} \times \mathcal{N}$ and the ℓth single-input-multiple-output (SIMO) channel path between S_k and the relay by $\tilde{h}_k(\ell) \triangleq [\tilde{h}_{k,1}(\ell), \ldots, \tilde{h}_{k,M}(\ell)]^T \in \mathbb{C}^{M \times 1}$. The transfer function corresponding to the nth sub-channel (subcarrier), $n \in \mathcal{N}$, is given by

$$h_k(n) \triangleq [h_{k,1}(n), \ldots, h_{k,M}(n)]^T = \sum_{\ell=0}^{L-1} \tilde{h}_k(\ell) e^{-j \frac{2\pi}{N} \ell n}, \tag{3}$$

where L is the number of propagation paths.

The block of information that S_k intends to send to D_k, defined by

$$x_k \triangleq [x_k(0) \quad \ldots \quad x_k(N-1)]^T \in \mathbb{C}^N, \tag{4}$$

is precoded by the inverse FFT (IFFT) as $\tilde{x}_k = F_N^H x_k$. Partition $\tilde{x}_k = \begin{bmatrix} \tilde{x}_{H,k} \\ \tilde{x}_{T,k} \end{bmatrix}$ with $\tilde{x}_{H,k} \in \mathbb{C}^{N-L}$ and $\tilde{x}_{T,k} \in \mathbb{C}^L$. In the first phase, S_k transmits the following cyclic-prefixed block of length $(N + L)$ to the relay:

$$\tilde{x}_k^{\mathrm{CP}} \triangleq \begin{bmatrix} \tilde{x}_{T,k} \\ \tilde{x}_{H,k} \\ \tilde{x}_{T,k} \end{bmatrix}. \tag{5}$$

By discarding the first L components of the received block and post-coding the last N components by the FFT F_N, we obtain the following received signal on the n-th subcarrier at the relay's m-th antenna with $m \in \mathcal{M} \triangleq \{1, \ldots, M\}$ and $n \in \mathcal{N}$:

$$y_m(n) = \sum_{k=1}^{K} h_{m,k}(n) x_k(n) + w_m(n), \tag{6}$$

where $w_m(n) \sim \mathcal{CN}(0, \sigma_R^2)$ is the background noise.

Next, assuming that $\tilde{\mathbf{g}}_k(\ell) \triangleq [\tilde{g}_{1,k}(\ell), \ldots, \tilde{g}_{M,k}(\ell)] \in \mathbb{C}^{1 \times M}$ is the ℓth multiple-input-single-output (MISO) channel

path between the relay and D_k, the transfer function corresponding to the nth sub-channel, $n \in \mathcal{N}$, is given by

$$g_k(n) \triangleq [g_{1,k}(n), \ldots, g_{M,k}(n)] = \sum_{\ell=0}^{L-1} \tilde{g}_u(\ell) e^{-j \frac{2\pi}{N} \ell n}. \tag{7}$$

In the second phase, for $y_m \triangleq [y_m(0), \ldots, y_m(N-1)]^T$, and $y \triangleq (y_1, \ldots, y_m)$, each $y_m(n)$ is amplified by $\mathbf{q}_m(n)$ to create the following block of length N

$$z_m \triangleq \begin{bmatrix} z_m(0) & \ldots & z_m(N-1) \end{bmatrix}^T$$
$$= \begin{bmatrix} \mathbf{q}_m(0) y_m(0) & \ldots & \mathbf{q}_m(N-1) y_m(N-1) \end{bmatrix}^T, \tag{8}$$

which is then precoded by the IFFT as $\tilde{z}_m \triangleq \begin{bmatrix} \tilde{z}_{H,m} \\ \tilde{z}_{T,m} \end{bmatrix} = F_N^H z_m$, $\tilde{z}_{H,m} \in \mathbb{C}^{N-L}$, $\tilde{z}_{T,m} \in \mathbb{C}^L$. It can be observed from (8) that using an equal number of transmit and receive antennas allows us to use an amplification vector (instead of an amplification matrix) at the relay for reducing the number of design variables. This is important in our setup, because in the presence of a large number of subcarriers in an OFDM based implementation, the number of design variables is already very large. Thus, our proposed setup simplifies the overall implementation and reduces the hardware cost.

By using the cyclic prefix $\tilde{z}_{T,m}$, the relay's m-th TA forwards the following OFDM block of length $(N + L)$ to all DNs: $\tilde{z}_m^{\mathrm{CP}} \triangleq \begin{bmatrix} \tilde{z}_{T,m} \\ \tilde{z}_{H,m} \\ \tilde{z}_{T,m} \end{bmatrix}$. Thus, the relay's average transmit power is[1]

$$\sum_{m=1}^{M} \mathbb{E} \left\{ \| \tilde{z}_m^{\mathrm{CP}} \|^2 \right\} = \left(1 + \frac{L}{N} \right) \sum_{m=1}^{M} \mathbb{E} \left\{ \| \tilde{z}_m \|^2 \right\} \tag{9}$$

$$= \sum_{m=1}^{M} \sum_{n=0}^{N-1} \left(1 + \frac{L}{N} \right) \mathbf{q}_m^2(n)$$

$$\times \left(\sum_{k=1}^{K} |h_{m,k}(n)|^2 |x_k(n)|^2 + \sigma_R^2 \right). \tag{10}$$

After discarding the L first components and post-coding the block of the last N components by FFT F_N, the signal received by D_k on the n-th subcarrier becomes

$$\hat{z}_k(n) = \sum_{m=1}^{M} g_{m,k}(n) z_m(n) + \nu_k(n) \tag{11}$$

$$= \sum_{m=1}^{M} g_{m,k}(n) \mathbf{q}_m(n) y_m(n) + \nu_k(n), \tag{12}$$

where $\nu_k(n) \sim \mathcal{CN}(0, \sigma^2)$ is the background noise.

B. Energy harvesting and recycling for powering the relay

Within the second phase, the energy source of Fig. 1 sends a dedicated energy signal to the relay. Let $\tilde{H}_E \in \mathbb{C}^{M \times M_E}$ be the frequency-flat time-domain MIMO channel matrix between

---

[1]For $z = (z_1, \ldots, z_N)^T$ with uncorrelated entries, it is true that each entry of its IFT transform has the power $\mathbb{E}(\|z\|^2)/N$ as each entry of $F_N^H(n', n)$ is of modulus $1/N$.

them and $\tilde{H}_{\text{LI}} \in \mathbb{C}^{M \times M}$ be the time-domain SI channel matrix at the relay. The time-domain signal received by the relay for harvesting energy during the second phase is given by

$$\tilde{y}_{\text{EH}}(n) = \tilde{H}_{\text{E}}\tilde{x}_{\text{EH}}(n) + \tilde{H}_{\text{LI}}\tilde{z}^{\text{CP}}(n) + \tilde{w}(n),$$

where $n \in \{0, \ldots, N + L - 1\}$, $\tilde{y}_{\text{EH}}(n) \triangleq \begin{bmatrix} \tilde{y}_{\text{EH},1}(n) \\ \ldots \\ \tilde{y}_{\text{EH},M}(n) \end{bmatrix}$,

$\tilde{x}_{\text{EH}}(n) \triangleq \begin{bmatrix} \tilde{x}_{\text{EH},1}(n) \\ \ldots \\ \tilde{x}_{\text{EH},M_E}(n) \end{bmatrix}$, $\tilde{z}^{\text{CP}}(n) \triangleq \begin{bmatrix} \tilde{z}_1^{\text{CP}}(n) \\ \ldots \\ \tilde{z}_M^{\text{CP}}(n) \end{bmatrix}$, and $\tilde{x}_{\text{EH}}(n)$ is

the time-domain energy signal transmitted by the energy node of Fig. 1. Using singular value decomposition of the channel matrix $\tilde{H}_{\text{E}}$ and transmit precoding, the power harvested at the relay (combined from all the receive antennas) is given by

$$e = \eta(N + L)\sigma_{\text{E}}\mathbf{p}_{\text{EH}} + \eta\gamma_{\text{LI}} \sum_{m=1}^{M} \sum_{n=0}^{N-1} \left(1 + \frac{L}{N}\right) \mathbf{q}_m^2(n)$$
$$\times \left(\sum_{k=1}^{K} |h_{m,k}(n)|^2 |x_k(n)|^2 + \sigma_R^2\right), \quad (13)$$

where η is the energy harvesting efficiency, σ_{E} is the maximal eigenvalue of $\tilde{H}_{\text{E}}\tilde{H}_{\text{E}}^H$, $\mathbf{p}_{\text{EH}}$ is the power allocated to transmit the energy signal and γ_{LI} is the SI path gain. In (13), we consider a linear EH model. The use of a non-linear EH model, which takes into account the fact that the energy conversion efficiency is a function of the power of the radio frequency (RF) signal received at the input of the EH circuit, is beyond the scope of this work, but may be explored in our future research.

III. Proper Gaussian signaling for OFDM relaying

Under PGS each x_k in (4) is proper Gaussian and represented by

$$x_k = \begin{bmatrix} \mathbf{p}_k(0)s_k(0) & \ldots & \mathbf{p}_k(N-1)s_k(N-1) \end{bmatrix}^T, \quad (14)$$

where $s_k(n) \in \mathcal{C}(0, 1)$ is the information symbol and $\mathbf{p}_k \triangleq \begin{bmatrix} \mathbf{p}_k(0) & \ldots & \mathbf{p}_k(N-1) \end{bmatrix}^T$ is the vector of power allocation.

The received signal (12) at D_k on the n-th subcarrier becomes

$$\hat{z}_k(n) = \sum_{m=1}^{M} g_{m,k}(n)\mathbf{q}_m(n)\left(\sum_{j=1}^{K} h_{m,j}(n)\mathbf{p}_j(n)s_j(n)\right.$$
$$\left. + w_m(n)\right) + \nu_k(n)$$
$$= \sum_{m=1}^{M} g_{m,k}(n)\mathbf{q}_m(n)h_{m,k}(n)\mathbf{p}_k(n)s_k(n)$$
$$+ \sum_{m=1}^{M} g_{m,k}(n)\mathbf{q}_m(n)w_m(n) + \sum_{m=1}^{M} g_{m,k}(n)\mathbf{q}_m(n)$$
$$\times \sum_{j\neq k}^{K} h_{m,j}(n)\mathbf{p}_j(n)s_j(n) + \nu_k(n)$$
$$= \alpha_{k,k}(\mathbf{q}(n))\mathbf{p}_k(n)s_k(n) + \sum_{m=1}^{M} g_{m,k}(n)\mathbf{q}_m(n)w_m(n)$$

$$+ \sum_{j\neq k}^{K} \alpha_{k,j}(\mathbf{q}(n))\mathbf{p}_j(n)s_j(n) + \nu_k(n), \quad (15)$$

where $\alpha_{k,j}(\mathbf{q}(n)) \triangleq \langle \mathbf{q}(n), \ell_{k,j}(n) \rangle \in \mathbb{C}$, for $\mathbf{q}(n) \triangleq \begin{bmatrix} \mathbf{q}_1(n) & \ldots & \mathbf{q}_M(n) \end{bmatrix}^T \in \mathbb{R}^M$, and

$$\ell_{k,j}(n) \triangleq \begin{bmatrix} g_{1,k}(n)h_{1,j}(n) & \ldots & g_{M,k}(n)h_{M,j}(n) \end{bmatrix}^T \in \mathbb{C}^M. \quad (16)$$

In what follows we also define $\mathbf{q} \triangleq \{\mathbf{q}(n) : n \in \mathcal{N}\}$, $\mathbf{p}(n) \triangleq \{\mathbf{p}_m(n) : m = 1, \ldots, M\}$ and $\mathbf{p} \triangleq \{\mathbf{p}(n) : n \in \mathcal{N}\}$.

The throughput of $s_k(n)$ at D_k is given by

$$r_{k,n}(\mathbf{p}(n), \mathbf{q}(n)) \triangleq \ln\left(1 + \frac{|\alpha_{k,k}(\mathbf{q}(n))|^2 \mathbf{p}_k^2(n)}{\phi_{k,n}(\mathbf{p}(n), \mathbf{q}(n))}\right), \quad (17)$$

where $\phi_{k,n}(\mathbf{p}(n), \mathbf{q}(n)) = \sum_{j\neq k}^{K} |\alpha_{k,j}(\mathbf{q}(n))|^2 \mathbf{p}_j^2(n) + \sigma_R^2 \sum_{m=1}^{M} |g_{m,k}(n)|^2 \mathbf{q}_m^2(n) + \sigma^2$.

Using (14), the relay's transmit power in (10) becomes

$$\left(1 + \frac{L}{N}\right) \sum_{m=1}^{M} \sum_{n=0}^{N-1} \mathbf{q}_m^2(n) \left(\sum_{k=1}^{K} |h_{m,k}(n)|^2 \mathbf{p}_k^2(n) + \sigma_R^2\right).$$

The power constraint at the relay is

$$\left(1 + \frac{L}{N}\right) \sum_{m=1}^{M} \sum_{n=0}^{N-1} \mathbf{q}_m^2(n) \left(\sum_{k=1}^{K} |h_{m,k}(n)|^2 \mathbf{p}_k^2(n) + \sigma_R^2\right) \leq$$
$$\eta \sum_{m=1}^{M} \sigma_{\text{E},m}\mathbf{p}_{\text{EH},m} + \eta\gamma_{\text{LI}}\left(1 + \frac{L}{N}\right) \sum_{m=1}^{M} \sum_{n=0}^{N-1} \mathbf{q}_m^2(n)$$
$$\times \left(\sum_{k=1}^{K} |h_{m,k}(n)|^2 |x_k(n)|^2 + \sigma_R^2\right). \quad (18)$$

Using (5), the transmit power of the source k is given by

$$\mathbb{E}\{\|\tilde{x}_k^{\text{CP}}\|^2\} = \left(1 + \frac{L}{N}\right) \mathbb{E}\{\|\tilde{x}_k\|^2\}$$
$$= \left(1 + \frac{L}{N}\right) \sum_{n=0}^{N-1} \mathbf{p}_k^2(n). \quad (19)$$

Therefore, the problem of sum-throughput maximization subject to both the power and EH constraints is formulated as

$$\max_{\mathbf{p}, \mathbf{p}_{\text{EH}}, \mathbf{q}} f(\mathbf{p}, \mathbf{q}) \triangleq \sum_{k=1}^{K} \sum_{n=0}^{N-1} r_{k,n}(\mathbf{p}(n), \mathbf{q}(n)) \quad (20a)$$

$$\text{s.t. } \left(1 + \frac{L}{N}\right) \sum_{k=1}^{K} \sum_{n=0}^{N-1} \mathbf{p}_k^2(n) + (N + L)\mathbf{p}_{\text{EH}} \leq P_{\text{T}}, \quad (20b)$$

$$\left(1 + \frac{L}{N}\right) \sum_{m=1}^{M} \sum_{n=0}^{N-1} \mathbf{q}_m^2(n) \left(\sum_{k=1}^{K} |h_{m,k}(n)|^2 \mathbf{p}_k^2(n)\right.$$
$$\left. + \sigma_R^2\right) \leq \bar{\eta}(N + L)\sigma_{\text{E}}\mathbf{p}_{\text{EH}}, \quad (20c)$$

where P_{T} is the combined power budget at the S and E nodes of Fig. 1, $\bar{\eta} = \eta/(1 - \eta\gamma_{\text{LI}})$, and the constraint (20c) is equivalent to the constraint (18).

At the optimal point, the inequality constraint (20b) is satisfied with the equality, i.e., $\mathbf{p}_{\text{EH}} =$

$\frac{1}{N+L}\left[P_T - \left(1+\frac{L}{N}\right)\sum_{k=1}^{K}\sum_{n=0}^{N-1}\mathbf{p}_k^2(n)\right]$, making the constraint (20c) equivalent to the following constraint

$$\sum_{m=1}^{M}\sum_{n=0}^{N-1}\mathbf{q}_m^2(n)\left(\sum_{k=1}^{K}|h_{m,k}(n)|^2\mathbf{p}_k^2(n)+\sigma_R^2\right)$$

$$+\bar{\eta}\sigma_E\sum_{k=1}^{K}\sum_{n=0}^{N-1}\mathbf{p}_k^2(n)\leq P_{tot} \quad (21)$$

for $P_{tot}\triangleq\bar{\eta}\sigma_E P_T/\left(1+\frac{L}{N}\right)$.

Thus, the problem (20) is actually the following problem

$$\max_{\mathbf{p},\mathbf{q}} f(\mathbf{p},\mathbf{q}) \quad \text{s.t.} \quad (21), \quad (22)$$

which is a large-scale nonconvex problem because the objective function in (22) is nonconcave, the constraint (21) is nonconvex, and the number of its decision variables is excessive since the number of subcarriers is up to thousands.

Let $(p^{(\kappa)},q^{(\kappa)})$ be the feasible point for (22) that is found from the $(\kappa-1)$-th round. By adopting the alternating descent technique, we first generate the next iterative point $p^{(\kappa+1)}$ with $\mathbf{q}$ held fixed at $q^{(\kappa)}$ and then the next iterative point $q^{(\kappa+1)}$ is generated with $\mathbf{p}$ held fixed at $p^{(\kappa+1)}$.

1) Alternating descent in $\mathbf{p}$: We aim for solving the following problem of alternating optimization in $\mathbf{p}$ to generate the next iterative point

$$\max_{\mathbf{p}} f(\mathbf{p},q^{(\kappa)})\triangleq\sum_{k=1}^{K}\sum_{n=0}^{N-1}r_{k,n}(\mathbf{p}(n),q^{(\kappa)}(n)) \quad \text{s.t.} \quad (23a)$$

$$\sum_{m=1}^{M}\sum_{n=0}^{N-1}\left(q_m^{(\kappa)}(n)\right)^2\left(\sum_{k=1}^{K}|h_{m,k}(n)|^2\mathbf{p}_k^2(n)+\sigma_R^2\right)$$

$$+\bar{\eta}\sigma_E\sum_{k=1}^{K}\sum_{n=0}^{N-1}\mathbf{p}_k^2(n)\leq P_{tot}, (23b)$$

where the constraint (23b) is convex quadratic, which is rewritten as

$$\sum_{k=1}^{K}\sum_{n=0}^{N-1}\nu_k^{(\kappa)}(n)\mathbf{p}_k^2(n)\leq P_{tot}^{(\kappa)}, \quad (24)$$

with $\nu_k^{(\kappa)}(n)\triangleq\bar{\eta}\sigma_E+\sum_{m=1}^{M}(q_m^{(\kappa)}(n))^2|h_{m,k}(n)|^2$, and $P_{tot}^{(\kappa)}\triangleq P_{tot}-\sigma_R^2\sum_{m=1}^{M}\sum_{n=0}^{N-1}\left(q_m^{(\kappa)}(n)\right)^2$.

Using the inequality (1) yields

$$r_{k,n}(\mathbf{p}(n),q^{(\kappa)}(n))\geq r_{k,n}^{(\kappa)}(\mathbf{p}(n)), \quad (25)$$

for $r_{k,n}^{(\kappa)}(\mathbf{p}(n))\triangleq a_k^{(\kappa)}(n)+2b_k^{(\kappa)}(n)\mathbf{p}_k(n)-\sum_{j=1}^{K}c_{k,j}^{(\kappa)}(n)\mathbf{p}_j^2(n)$

with

$$a_k^{(\kappa)}(n)\triangleq r_{k,n}(p^{(\kappa)},q^{(\kappa)})-\frac{\chi_k^{(\kappa)}(n)}{\psi_k^{(\kappa)}(n)}$$

$$-\frac{\chi_k^{(\kappa)}(n)\left(\sigma_R^2\sum_{m=1}^{M}|g_{m,k}(n)|^2\left(q_m^{(\kappa)}(n)\right)^2+\sigma^2\right)}{\psi_k^{(\kappa)}(n)(\psi_k^{(\kappa)}(n)+\chi_k^{(\kappa)}(n))},$$

$$b_k^{(\kappa)}(n)\triangleq\frac{|\alpha_{k,k}(q^{(\kappa)}(n))|^2 p_k^{(\kappa)}(n)}{\psi_k^{(\kappa)}(n)},$$

$$c_{k,j}^{(\kappa)}(n)\triangleq\frac{\chi_k^{(\kappa)}(n)}{\psi_k^{(\kappa)}(n)(\psi_k^{(\kappa)}(n)+\chi_k^{(\kappa)}(n))}|\alpha_{k,j}(q^{(\kappa)}(n))|^2,$$

$$\chi_k^{(\kappa)}(n)\triangleq|\alpha_{k,k}(q^{(\kappa)}(n))|^2\left(p_k^{(\kappa)}(n)\right)^2, \text{ and}$$

$$\psi_k^{(\kappa)}(n)\triangleq\sum_{j\neq k}^{K}\left|\alpha_{k,j}(q^{(\kappa)}(n))\right|^2\left(p_j^{(\kappa)}(n)\right)^2$$

$$+\sigma_R^2\sum_{m=1}^{M}|g_{m,k}(n)|^2\left(q_m^{(\kappa)}(n)\right)^2+\sigma^2.$$

For

$$f^{(\kappa)}(\mathbf{p}) \triangleq \sum_{k=1}^{K}\sum_{n=0}^{N-1}r_{k,n}^{(\kappa)}(\mathbf{p}(n))$$

$$= \sum_{k=1}^{K}\sum_{n=0}^{N-1}\left(a_k^{(\kappa)}(n)+2b_k^{(\kappa)}(n)\mathbf{p}_k(n)\right.$$

$$\left.-d_k^{(\kappa)}(n)\mathbf{p}_k^2(n)\right), \quad (26)$$

with $d_k^{(\kappa)}(n)\triangleq\sum_{j=1}^{K}c_{j,k}^{(\kappa)}(n)$, it may be readily checked that $f(\mathbf{p},q^{(\kappa)})=f^{(\kappa)}(\mathbf{p})\,\forall\,\mathbf{p}$ and $f(p^{(\kappa)},q^{(\kappa)})\geq f^{(\kappa)}(p^{(\kappa)})$, so $f^{(\kappa)}(\mathbf{p})$ is a tight concave quadratic minorant of $f(\mathbf{p},q^{(\kappa)})$ [40]. We solve the following convex quadratic problem of minorant maximization at the κ-th iteration to generate $p^{(\kappa+1)}$:

$$\max_{\mathbf{p}} f^{(\kappa)}(\mathbf{p}) \quad \text{s.t.} \quad (24). \quad (27)$$

The problem (27) admits the closed form solution:

$$p_k^{(\kappa+1)}(n)=$$

$$\begin{cases} \dfrac{b_k^{(\kappa)}(n)}{d_k^{(\kappa)}(n)} & \text{if } \sum_{k=1}^{K}\sum_{n=0}^{N-1}\nu_k^{(\kappa)}(n)\left(\dfrac{b_k^{(\kappa)}(n)}{d_k^{(\kappa)}(n)}\right)^2\leq P_{tot}^{(\kappa)} \\ \dfrac{b_k^{(\kappa)}(n)}{d_k^{(\kappa)}(n)+\mu\nu_k^{(\kappa)}(n)} & \text{otherwise,} \end{cases}$$

$$(28)$$

where $\mu>0$ is found by bisection such that

$$\sum_{k=1}^{K}\sum_{n=0}^{N-1}\nu_k^{(\kappa)}(n)\left(\frac{b_k^{(\kappa)}(n)}{d_k^{(\kappa)}(n)+\mu\nu_k^{(\kappa)}(n)}\right)^2=P_{tot}^{(\kappa)}.$$

Note that $f^{(\kappa)}(p^{(\kappa+1)})>f^{(\kappa)}(p^{(\kappa)})=f(p^{(\kappa)},q^{(\kappa)})$ because $p^{(\kappa+1)}$ and $p^{(\kappa)}$ are the optimal solution and a feasible point for (27). We thus arrive at

$$f(p^{(\kappa+1)},q^{(\kappa)})\geq f^{(\kappa)}(p^{(\kappa+1)})>f(p^{(\kappa)},q^{(\kappa)}), \quad (29)$$

i.e. $(p^{(\kappa+1)},q^{(\kappa)})$ is a better feasible point than $(p^{(\kappa)},q^{(\kappa)})$ for (20).

2) Alternating descent in $\mathbf{q}$: Next, we aim for solving the following problem of alternating optimization in $\mathbf{q}$ to generate the next iterative point $q^{(\kappa+1)}$:

$$\max_{\mathbf{q}} f(p^{(\kappa+1)},\mathbf{q})\triangleq\sum_{k=1}^{K}\sum_{n=0}^{N-1}r_{k,n}(p^{(\kappa+1)}(n),\mathbf{q}(n)) \quad (30a)$$

$$\text{s.t.} \sum_{m=1}^{M}\sum_{n=0}^{N-1}(\mathbf{q}_m(n))^2\left(\sum_{k=1}^{K}|h_{m,k}(n)|^2(p_k^{(\kappa+1)}(n))^2\right.$$

$$+\sigma_R^2\Big) + \bar{\eta}\sigma_E \sum_{k=1}^{K}\sum_{n=0}^{N-1}(p_k^{(\kappa+1)}(n))^2 \leq P_{tot}. \quad (30b)$$

Let us rewrite (30b) as

$$\sum_{n=0}^{N-1}(\mathbf{q}(n))^T\Theta^{(\kappa)}(n)\mathbf{q}(n) \leq \tilde{P}_{tot}^{(\kappa)}, \quad (31)$$

with $\tilde{P}_{tot}^{(\kappa)} \triangleq P_{tot} - \bar{\eta}\sigma_E \sum_{k=1}^{K}\sum_{n=0}^{N-1}(p_k^{(\kappa+1)}(n))^2$, and

$$\Theta^{(\kappa)}(n) \triangleq \mathsf{diag}\left[\sum_{k=1}^{K}|h_{m,k}(n)|^2(p_k^{(\kappa+1)}(n))^2 + \sigma_R^2\right]_{m=1,\dots,M}.$$

Using the inequality (1) yields

$$r_{k,n}(p^{(\kappa+1)}(n),\mathbf{q}(n)) \geq \tilde{r}_{k,n}^{(\kappa)}(\mathbf{q}(n)), \quad (32)$$

where $\tilde{r}_{k,n}^{(\kappa)}(\mathbf{q}(n)) \triangleq \tilde{a}_k^{(\kappa)}(n) + 2\langle\tilde{b}_k^{(\kappa)}(n),\mathbf{q}(n)\rangle - (\mathbf{q}(n))^T\tilde{C}_k^{(\kappa)}(n)\mathbf{q}(n)$, with

$$\tilde{a}_k^{(\kappa)}(n) \triangleq \tilde{r}_{k,n}(q^{(\kappa)}(n)) - \frac{\tilde{\chi}_k^{(\kappa)}(n)}{\tilde{\psi}_k^{(\kappa)}(n)}$$
$$-\frac{\tilde{\chi}_k^{(\kappa)}(n)}{\tilde{\psi}_k^{(\kappa)}(n)(\tilde{\psi}_k^{(\kappa)}(n) + \tilde{\chi}_k^{(\kappa)}(n))}\sigma^2,$$

$$\tilde{b}_k^{(\kappa)}(n) \triangleq \frac{|\alpha_{k,k}(q^{(\kappa)}(n))|(p_k^{(\kappa+1)}(n))^2}{\tilde{\psi}_k^{(\kappa)}(n)}\Re\{\ell_{k,k}(n)\} \in \mathbb{R}^M,$$

$$\tilde{C}_k^{(\kappa)}(n) \triangleq \sum_{j=1}^{K}\left(\frac{\tilde{\chi}_k^{(\kappa)}(n)(p_j^{(\kappa+1)}(n))^2}{\tilde{\psi}_k^{(\kappa)}(n)(\tilde{\psi}_k^{(\kappa)}(n) + \tilde{\chi}_k^{(\kappa)}(n))}\right.$$
$$\left.\times\left([\Re\{\ell_{k,j}(n)\}]^2 + [\Im\{\ell_{k,j}(n)\}]^2\right)\right)$$
$$+\frac{\sigma_R^2\tilde{\chi}_k^{(\kappa)}(n)}{\tilde{\psi}_k^{(\kappa)}(n)(\tilde{\psi}_k^{(\kappa)}(n) + \tilde{\chi}_k^{(\kappa)}(n))}$$
$$\times\mathsf{diag}\left[|g_{m,k}(n)|^2\right]_{m=1,\dots,M}$$
$$\succeq 0,$$

and $\tilde{\chi}_k^{(\kappa)}(n) \triangleq |\alpha_{k,k}(q^{(\kappa)}(n))|^2(p_k^{(\kappa+1)}(n))^2$, and $\tilde{\psi}_k^{(\kappa)}(n) \triangleq \sum_{j\neq k}^{K}|\alpha_{k,j}(q^{(\kappa)}(n))|^2(p_j^{(\kappa+1)}(n))^2 + \sigma_R^2\sum_{m=1}^{M}|g_{m,k}(n)|^2(q_m^{(\kappa)}(n))^2 + \sigma^2$.

Again, it may then be readily checked that the following function $\tilde{f}^{(\kappa)}(\mathbf{q})$ serves as a tight concave quadratic minorant of the nonconcave function $f(p^{(\kappa+1)},\mathbf{q})$:

$$\tilde{f}^{(\kappa)}(\mathbf{q}) \triangleq \sum_{k=1}^{K}\sum_{n=0}^{N-1}\tilde{r}_{k,n}^{(\kappa)}(\mathbf{q}(n))$$
$$= \sum_{n=0}^{N-1}\Big(\tilde{a}^{(\kappa)}(n) + 2\langle\tilde{b}^{(\kappa)}(n),\mathbf{q}(n)\rangle$$
$$-(\mathbf{q}(n))^T\tilde{C}^{(\kappa)}(n)\mathbf{q}(n)\Big) \quad (33)$$

with $\tilde{a}^{(\kappa)}(n) \triangleq \sum_{k=1}^{K}\tilde{a}_k^{(\kappa)}(n)$, $\tilde{b}^{(\kappa)}(n) \triangleq \sum_{k=1}^{K}\tilde{b}_k^{(\kappa)}(n)$, and $\tilde{C}^{(\kappa)}(n) \triangleq \sum_{k=1}^{K}\tilde{C}_k^{(\kappa)}(n)$.

Algorithm 1 Resource allocation algorithm for PGS based Problem (22)

1: **Initialization**: Randomly generate $(p^{(0)},q^{(0)},)$ satisfying the constraint (21). Set $\kappa := 0$.
2: **Repeat until convergence of the objective function in** (22): Update $p^{(\kappa+1)}$ using (28) and then update $q^{(\kappa+1)}$ using (35). Reset $\kappa \leftarrow \kappa + 1$.

We thus solve the following convex quadratic problem of minorant maximization to generate the next iterative point $q^{(\kappa+1)}$:

$$\max_{\mathbf{q}} \tilde{f}^{(\kappa)}(\mathbf{q}) \quad \text{s.t.} \quad (31). \quad (34)$$

This problem admits the following closed-form solution:

$$q^{(\kappa+1)}(n) =$$
$$\begin{cases} (\tilde{C}^{(\kappa)}(n))^{-1}\tilde{b}^{(\kappa)}(n) & \text{if } \Xi^{(\kappa)} \leq \tilde{P}_{tot}^{(\kappa)} \\ (\tilde{C}^{(\kappa)}(n) + \mu\Theta^{(\kappa)}(n))^{-1}\tilde{b}^{(\kappa)}(n) & \text{otherwise,} \end{cases}$$
$$(35)$$

where

$$\Xi^{(\kappa)} \triangleq \sum_{n=0}^{N-1}||(\Theta^{(\kappa)}(n))^{1/2}(\tilde{C}^{(\kappa)}(n))^{-1}\tilde{b}^{(\kappa)}(n)||^2$$

and μ is found by bisection for ensuring that $\sum_{n=0}^{N-1}||(\Theta^{(\kappa)}(n))^{1/2}(\tilde{C}^{(\kappa)}(n) + \mu\Theta^{(\kappa)}(n))^{-1}\tilde{b}^{(\kappa)}(n)||^2 = \tilde{P}_{tot}^{(\kappa)}$.

Using a similar argument as that for proving (29), we can show that

$$f(p^{(\kappa+1)},q^{(\kappa+1)}) > f(p^{(\kappa+1)},q^{(\kappa)}), \quad (36)$$

which together with (29) show that $(p^{(\kappa+1)},q^{(\kappa+1)})$ is a better feasible point than $(p^{(\kappa)},q^{(\kappa)})$ for (20). Algorithm 1 provides the pseudo-code for the alternating descent procedure based on the closed-form expressions of (28) and (35). According to [36], such an algorithm often converges at least to a locally optimal solution of (22).

IV. IMPROPER GAUSSIAN SIGNALING FOR OFDM RELAYING

Under IGS, each $x_k(n)$ in (4) is improper Gaussian as it is represented by

$$x_k(n) = \mathbf{v}_{k,1}(n)s_k(n) + \mathbf{v}_{k,2}(n)s_k^*(n), \quad \mathbf{v}_{k,i} \in \mathbb{C}, i = 1, 2. \quad (37)$$

Note that $x_k(n)$ defined by (14) is restricted on the one-dimensional manifold $\mathbb{E}(|\Re\{x_k(n)\}|^2) = \mathbb{E}(|\Im\{x_k(n)\}|^2)$. In contrast, $x_k(n)$ defined by (37) is restricted on a two-dimensional manifold as it is immediate to check that $\mathbb{E}(|\Re\{x_k(n)\}|^2) \neq \mathbb{E}(|\Im\{x_k(n)\}|^2)$. As such, the so called widely-linear operator applied to $s_k(n)$ in (37) augments its dimensionality, providing more degrees of signaling freedoms.

Then the received signal (12) at D_k on the n-th subcarrier is

$$\hat{z}_k(n) = \sum_{m=1}^{M}g_{m,k}(n)\mathbf{q}_m(n)\left(\sum_{j=1}^{K}h_{m,j}(n)\left(\mathbf{v}_{j,1}(n)s_j(n)\right.\right.$$

$$+ \mathbf{v}_{j,2}(n)s_j^*(n)) + w_m(n)\Big) + \nu_k(n)$$

$$= \sum_{j=1}^{K} \alpha_{k,j}(\mathbf{q}(n))\left(\mathbf{v}_{j,1}(n)s_j(n) + \mathbf{v}_{j,2}(n)s_j^*(n)\right)$$

$$+ \sum_{m=1}^{M} g_{m,k}(n)\mathbf{q}_m(n)w_m(n) + \nu_k(n). \tag{38}$$

In what follows, we use the following notations:

$$\bar{z}_k(n) \triangleq \begin{bmatrix} \Re\{\hat{z}_k(n)\} \\ \Im\{\hat{z}_k(n)\} \end{bmatrix}, \bar{s}_k(n) \triangleq \begin{bmatrix} \Re\{s_k(n)\} \\ \Im\{s_k(n)\} \end{bmatrix},$$

$$\bar{w}_m(n) \triangleq \begin{bmatrix} \Re\{w_m(n)\} \\ \Im\{w_m(n)\} \end{bmatrix}, \bar{\nu}_k(n) \triangleq \begin{bmatrix} \Re\{\nu_k(n)\} \\ \Im\{\nu_k(n)\} \end{bmatrix},$$

$$G_{m,k}(n) \triangleq \begin{bmatrix} \Re\{g_{m,k}(n)\} & -\Im\{g_{m,k}(n)\} \\ \Im\{g_{m,k}(n)\} & \Re\{g_{m,k}(n)\} \end{bmatrix},$$

$$\mathbf{V}_j(n) \triangleq \begin{bmatrix} \Re\{\mathbf{v}_{j,1}(n) + \mathbf{v}_{j,2}(n)\} & -\Im\{\mathbf{v}_{j,1}(n) - \mathbf{v}_{j,2}(n)\} \\ \Im\{\mathbf{v}_{j,1}(n) + \mathbf{v}_{j,2}(n)\} & \Re\{\mathbf{v}_{j,1}(n) - \mathbf{v}_{j,2}(n)\} \end{bmatrix},$$

and

$$\mathcal{L}_{k,j}(\mathbf{q}(n)) \triangleq \begin{bmatrix} \Re\{\alpha_{k,j}(\mathbf{q}(n))\} & -\Im\{\alpha_{k,j}(\mathbf{q}(n))\} \\ \Im\{\alpha_{k,j}(\mathbf{q}(n))\} & \Re\{\alpha_{k,j}(\mathbf{q}(n))\} \end{bmatrix}$$

$$= \begin{bmatrix} \Re\{\ell_{k,j}^T(n)\}\mathbf{q}(n) & -\Im\{\ell_{k,j}^T(n)\}\mathbf{q}(n) \\ \Im\{\ell_{k,j}^T(n)\}\mathbf{q}(n) & \Re\{\ell_{k,j}^T(n)\}\mathbf{q}(n) \end{bmatrix}, \tag{39}$$

where $\ell_{k,j}(n)$ is defined from (16). It may be readily shown that $\mathbb{E}\{[\bar{s}_k(n)]^2\} = \frac{1}{2}I_2$, $\mathbb{E}\{[\bar{w}_m(n)]^2\} = \frac{1}{2}\sigma_R^2 I_2$, $\mathbb{E}\{[\bar{\nu}_k(n)]^2\} = \frac{1}{2}\sigma^2 I_2$.

The equivalent real composite form of (38) is

$$\bar{z}_k(n) = \sum_{j=1}^{K} \mathcal{L}_{k,j}(\mathbf{q}(n))\mathbf{V}_j(n)\bar{s}_j(n)$$

$$+ \sum_{m=1}^{M} \mathbf{q}_m(n)G_{m,k}(n)\bar{w}_m(n) + \bar{\nu}_k(n) \tag{40}$$

$$= \sum_{j=1}^{K} \mathcal{L}_{k,j}(\mathbf{q}(n))\mathbf{P}_j(n)\bar{s}_j(n)$$

$$+ \sum_{m=1}^{M} \mathbf{q}_m(n)G_{m,k}(n)\bar{w}_m(n) + \bar{\nu}_k(n) \tag{41}$$

under the variable change

$$\mathbf{P}_j(n) \triangleq \begin{bmatrix} \mathbf{p}_j^{11}(n) & \mathbf{p}_j^{12}(n) \\ \mathbf{p}_j^{21}(n) & \mathbf{p}_j^{22}(n) \end{bmatrix}$$

$$= \begin{bmatrix} \Re\{\mathbf{v}_{j,1}(n) + \mathbf{v}_{j,2}(n)\} & -\Im\{\mathbf{v}_{j,1}(n) - \mathbf{v}_{j,2}(n)\} \\ \Im\{\mathbf{v}_{j,1}(n) + \mathbf{v}_{j,2}(n)\} & \Re\{\mathbf{v}_{j,1}(n) - \mathbf{v}_{j,2}(n)\} \end{bmatrix}, \tag{42}$$

which is invertible:

$$\boldsymbol{V}_j(n) \triangleq \begin{bmatrix} \Re\{\mathbf{v}_{j,1}(n)\} & \Im\{\mathbf{v}_{j,1}(n)\} \\ \Re\{\mathbf{v}_{j,2}(n)\} & \Im\{\mathbf{v}_{j,2}(n)\} \end{bmatrix}$$

$$= \frac{1}{2}\begin{bmatrix} \mathbf{p}_j^{11}(n) + \mathbf{p}_j^{22}(n) & \mathbf{p}_j^{21}(n) - \mathbf{p}_j^{12}(n) \\ \mathbf{p}_j^{11}(n) - \mathbf{p}_j^{22}(n) & \mathbf{p}_j^{21}(n) + \mathbf{p}_j^{12}(n) \end{bmatrix}. \tag{43}$$

Furthermore, we have:

$$||\boldsymbol{V}_j(n)||^2 = \langle[\boldsymbol{V}_j(n)]^2\rangle = \frac{1}{2}||\mathbf{P}_j(n)||^2 = \frac{1}{2}\langle[\mathbf{P}_j(n)]^2\rangle. \tag{44}$$

and the relay's transmit power is

$$\sum_{m=1}^{M}\sum_{n=0}^{N-1} \bar{L}\mathbf{q}_m^2(n)\left(\frac{1}{2}\sum_{k=1}^{K}\langle[H_{m,k}^T(n)]^2, [\mathbf{P}_k(n)]^2\rangle + \sigma_R^2\right), \tag{45}$$

for $\bar{L} = 1 + \frac{L}{N}$ and

$$H_{m,k}(n) \triangleq \begin{bmatrix} \Re\{h_{m,k}(n)\} & -\Im\{h_{m,k}(n)\} \\ \Im\{h_{m,k}(n)\} & \Re\{h_{m,k}(n)\} \end{bmatrix}.$$

Thus, the throughput of $s_k(n)$ is given by $(1/2)\rho_{k,n}(\mathbf{P}(n), \mathbf{q}(n))$ [41] with

$$\rho_{k,n}(\mathbf{P}(n), \mathbf{q}(n)) =$$

$$\ln\left|I_2 + [\mathcal{L}_{k,k}(\mathbf{q}(n))\mathbf{P}_k(n)]^2\left(\sum_{j\neq k}^{K}[\mathcal{L}_{k,j}(\mathbf{q}(n))\mathbf{P}_j(n)]^2\right.\right.$$

$$\left.\left. + \sigma_R^2\sum_{m=1}^{M}\mathbf{q}_m^2(n)[G_{m,k}(n)]^2 + \sigma^2 I_2\right)^{-1}\right|. \tag{46}$$

Based on (45), the problem of IGS sum-throughput maximization, corresponding to its dual PGS pair (22), is formulated as:

$$\max_{\mathbf{P},\mathbf{q}} F(\mathbf{P},\mathbf{q}) \triangleq \frac{1}{2}\sum_{k=1}^{K}\sum_{n=0}^{N-1}\rho_{k,n}(\mathbf{P}(n), \mathbf{q}(n)) \tag{47a}$$

$$\text{s.t.} \quad \sum_{m=1}^{M}\sum_{n=0}^{N-1}\mathbf{q}_m^2(n)\left(\frac{1}{2}\sum_{k=1}^{K}\langle[H_{m,k}^T(n)]^2, [\mathbf{P}_k(n)]^2\rangle\right.$$

$$\left. + \sigma_R^2\right) + \frac{1}{2}\bar{\eta}\sigma_E\sum_{k=1}^{K}\sum_{n=0}^{N-1}\langle[\mathbf{P}_k(n)]^2\rangle \leq P_{tot}, \tag{47b}$$

for P_{tot} defined after (18). As for PGS, we aim for developing the corresponding alternating decent iterations, which are based on closed form expressions.

Let $(P^{(\kappa)}, q^{(\kappa)})$ be the feasible point of (47) that is found from the $(\kappa - 1)$-th iteration.

A. Alternating descent in $\mathbf{P}$

To generate $P^{(\kappa+1)}$ we consider the following problem of alternating optimization in $\mathbf{P}$ with $\mathbf{q}$ held fixed at $q^{(\kappa)}$:

$$\max_{\mathbf{P}} F(\mathbf{P}, q^{(\kappa)}) \triangleq \frac{1}{2}\sum_{k=1}^{K}\sum_{n=0}^{N-1}\rho_{k,n}(\mathbf{P}(n), q^{(\kappa)}(n)) \tag{48a}$$

$$\text{s.t.} \quad \sum_{m=1}^{M}\sum_{n=0}^{N-1}(q_m^{(\kappa)}(n))^2\left(\frac{1}{2}\sum_{k=1}^{K}\langle[H_{m,k}^T(n)]^2, [\mathbf{P}_k(n)]^2\rangle\right.$$

$$\left. + \sigma_R^2\right) + \frac{1}{2}\bar{\eta}\sigma_E\sum_{k=1}^{K}\sum_{n=0}^{N-1}\langle[\mathbf{P}_k(n)]^2\rangle \leq P_{tot}. \tag{48b}$$

The constraint (48b) is simplified to

$$\sum_{k=1}^{K}\sum_{n=0}^{N-1}\langle\mathcal{N}_k^{(\kappa)}(n), [\mathbf{P}_k(n)]^2\rangle \leq P_{tot}^{(\kappa)}, \tag{49}$$

with $\mathcal{N}_k^{(\kappa)}(n) \triangleq \frac{1}{2}\left(\bar{\eta}\sigma_E I_2 + \sum_{m=1}^{M}(q_m^{(\kappa)}(n))^2[H_{m,k}^T(n)]^2\right)$, and $P_{tot}^{(\kappa)} \triangleq P_{tot} - \sigma_R^2\sum_{m=1}^{M}\sum_{n=0}^{N-1}\left(q_m^{(\kappa)}(n)\right)^2$.

Recalling that $\rho_{k,n}(\mathbf{P}(n), q^{(\kappa)}(n)) \triangleq \ln\Big|I_2 +$

$[\mathcal{L}_{k,k}(q^{(\kappa)}(n))\mathbf{P}_k(n)]^2 \Big(\sum_{j\neq k}^{K}[\mathcal{L}_{k,j}(q^{(\kappa)}(n))\mathbf{P}_j(n)]^2 +$

$\sigma_R^2 \sum_{m=1}^{M}(q_m^{(\kappa)}(n))^2[G_{m,k}(n)]^2 + \sigma^2 I_2\Big)^{-1}\Big|$, we use the

inequality (2) to obtain

$$\rho_{k,n}(\mathbf{P}(n), q^{(\kappa)}(n)) \geq \rho_{k,n}^{(\kappa)}(\mathbf{P}(n)) \tag{50}$$

for $\rho_{k,n}^{(\kappa)}(\mathbf{P}(n)) \triangleq a_k^{(\kappa)}(n) + 2\langle B_k^{(\kappa)}(n), \mathbf{P}_k(n)\rangle -$
$\sum_{j=1}^{K}\langle C_{k,j}^{(\kappa)}(n), [\mathbf{P}_j(n)]^2\rangle$, with

$$
\begin{aligned}
a_k^{(\kappa)}(n) &\triangleq \rho_{k,n}(P^{(\kappa)}(n), q^{(\kappa)}(n)) \\
&\quad -\langle(\Psi_k^{(\kappa)}(n))^{-1}, [\mathcal{L}_{k,k}(q^{(\kappa)}(n))P_k^{(\kappa)}(n)]^2\rangle \\
&\quad -\langle\Phi_k^{(\kappa)}(n), \sigma_R^2 \sum_{m=1}^{M}(q_m^{(\kappa)}(n))^2[G_{m,k}(n)]^2 + \sigma^2 I_2\rangle, \\
B_k^{(\kappa)}(n) &\triangleq (\mathcal{L}_{k,k}(q^{(\kappa)}(n)))^T(\Psi_k^{(\kappa)}(n))^{-1} \\
&\quad \times \mathcal{L}_{k,k}(q^{(\kappa)}(n))P_k^{(\kappa)}(n), \\
C_{k,j}^{(\kappa)}(n) &\triangleq (\mathcal{L}_{k,j}(q^{(\kappa)}(n)))^T \Phi_k^{(\kappa)}(n)\mathcal{L}_{k,j}(q^{(\kappa)}(n)),
\end{aligned}
$$

and

$$
\begin{aligned}
\Psi_k^{(\kappa)}(n) &\triangleq \sum_{j\neq k}^{K}[\mathcal{L}_{k,j}(q^{(\kappa)}(n))P_j^{(\kappa)}(n)]^2 \\
&\quad +\sigma_R^2 \sum_{m=1}^{M}(q_m^{(\kappa)}(n))^2[G_{m,k}(n)]^2 + \sigma^2 I_2, \\
\Phi_k^{(\kappa)}(n) &\triangleq (\Psi_k^{(\kappa)}(n))^{-1} - (\Psi_k^{(\kappa)}(n) \\
&\quad +[\mathcal{L}_{k,k}(q^{(\kappa)}(n))P_k^{(\kappa)}(n)]^2)^{-1}
\end{aligned}
$$

Therefore, the function $F^{(\kappa)}(\mathbf{P})$ below provides a tight concave quadratic minorant of the nonconcave function $F(\mathbf{P}, q^{(\kappa)})$:

$$
\begin{aligned}
F^{(\kappa)}(\mathbf{P}) &\triangleq \frac{1}{2}\sum_{k=1}^{K}\sum_{n=0}^{N-1}\rho_{k,n}^{(\kappa)}(\mathbf{P}(n)) \\
&= \frac{1}{2}\sum_{k=1}^{K}\sum_{n=0}^{N-1}\Big(a_k^{(\kappa)}(n) + 2\langle B_k^{(\kappa)}(n), \mathbf{P}_k(n)\rangle \\
&\quad -\langle D_k^{(\kappa)}(n), [\mathbf{P}_k(n)]^2\rangle\Big),
\end{aligned} \tag{51}
$$

with $D_k^{(\kappa)}(n) \triangleq \sum_{j=1}^{K}C_{j,k}^{(\kappa)}(n)$.

We solve the following convex quadratic problem of minorant maximization at the κ-th iteration to generate $P^{(\kappa+1)}$:

$$\max_{\mathbf{P}} F^{(\kappa)}(\mathbf{P}) \quad \text{s.t. (49).} \tag{52}$$

This problem admits the closed form solution of

$$
P_k^{(\kappa+1)}(n) =
\begin{cases}
(D_k^{(\kappa)}(n))^{-1}B_k^{(\kappa)}(n) & \text{if } \Xi^{(\kappa)} \leq P_{tot}^{(\kappa)} \\
(D_k^{(\kappa)}(n) + \mu\mathcal{N}_k^{(\kappa)}(n))^{-1}B_k^{(\kappa)}(n) & \text{otherwise,}
\end{cases} \tag{53}
$$

where

$$\Xi^{(\kappa)} \triangleq \sum_{k=1}^{K}\sum_{n=0}^{N-1}\langle\mathcal{N}_k^{(\kappa)}(n), [(D_k^{(\kappa)}(n))^{-1}B_k^{(\kappa)}(n)]^2\rangle$$

and μ is found by bisection such that

$$\sum_{k=1}^{K}\sum_{n=0}^{N-1}\langle\mathcal{N}_k^{(\kappa)}(n), [(D_k^{(\kappa)}(n)+\mu\mathcal{N}_k^{(\kappa)}(n))^{-1}B_k^{(\kappa)}(n)]^2\rangle = P_{tot}^{(\kappa)}.$$

Similarly to (29), we can show that $(P^{(\kappa+1)}, q^{(\kappa)})$ is a better feasible point than $(P^{(\kappa)}, q^{(\kappa)})$ for (47) because

$$F(P^{(\kappa+1)}, q^{(\kappa)}) > F(P^{(\kappa)}, q^{(\kappa)}). \tag{54}$$

B. Alternating descent in $\mathbf{q}$

Next, we aim for addressing the following alternating optimization in $\mathbf{q}$ with $\mathbf{P}$ held fixed at $P^{(\kappa+1)}$ to generate the next iterative point $q^{(\kappa+1)}$:

$$\max_{\mathbf{q}} \; F(P^{(\kappa+1)}, \mathbf{q}) \triangleq \frac{1}{2}\sum_{k=1}^{K}\sum_{n=0}^{N-1}\rho_{k,n}(P^{(\kappa+1)}(n), \mathbf{q}(n)) \tag{55a}$$

$$
\begin{aligned}
\text{s.t.} \quad &\sum_{m=1}^{M}\sum_{n=0}^{N-1}\mathbf{q}_m^2(n)\Big(\frac{1}{2}\sum_{k=1}^{K}\langle[H_{m,k}^T(n)]^2, [P_k^{(\kappa+1)}(n)]^2\rangle \\
&+\sigma_R^2\Big) + \frac{1}{2}\bar{\eta}\sigma_E\sum_{k=1}^{K}\sum_{n=0}^{N-1}\langle[P_k^{(\kappa+1)}(n)]^2\rangle \leq P_{tot}
\end{aligned} \tag{55b}
$$

where $\rho_{k,n}(P^{(\kappa+1)}(n), \mathbf{q}(n)) = \ln\Big|I_2 +$

$[\mathcal{L}_{k,k}(\mathbf{q}(n))P_k^{(\kappa+1)}(n)]^2\Big(\sum_{j\neq k}^{K}[\mathcal{L}_{k,j}(\mathbf{q}(n))P_j^{(\kappa+1)}(n)]^2 +$

$\sigma_R^2\sum_{m=1}^{M}\mathbf{q}_m^2(n)[G_{m,k}(n)]^2 + \sigma^2 I_2\Big)^{-1}\Big|$.

Let us now rewrite (55b) as

$$\sum_{n=0}^{N-1}(\mathbf{q}(n))^T\tilde{\Theta}^{(\kappa)}(n)\mathbf{q}(n) \leq \tilde{P}_{tot}^{(\kappa)}, \tag{56}$$

with $\tilde{\Theta}^{(\kappa)}(n) \triangleq \text{diag}\Big[\frac{1}{2}\sum_{k=1}^{K}\langle[H_{m,k}^T(n)]^2, [P_k^{(\kappa+1)}(n)]^2\rangle +$
$\sigma_R^2\Big]_{m=1,\dots,M}$, and $\tilde{P}_{tot}^{(\kappa)} \triangleq P_{tot} -$
$\frac{1}{2}\bar{\eta}\sigma_E\sum_{k=1}^{K}\sum_{n=0}^{N-1}\langle[P_k^{(\kappa+1)}(n)]^2\rangle$.

Then using the inequality (2) yields

$$
\begin{aligned}
&\rho_{k,n}(P^{(\kappa+1)}(n), \mathbf{q}(n)) \\
&\geq \tilde{\rho}_{k,n}^{(\kappa)}(\mathbf{q}(n)) \\
&\triangleq \tilde{a}_k^{(\kappa)}(n) + 2\langle\tilde{B}_k^{(\kappa)}(n), \mathcal{L}_{k,k}(\mathbf{q}(n))\rangle \\
&\quad -\sum_{j=1}^{K}\langle\tilde{\Phi}_k^{(\kappa)}(n), [\mathcal{L}_{k,j}(\mathbf{q}(n))P_j^{(\kappa)}(n)]^2\rangle \\
&\quad -\sigma_R^2\sum_{m=1}^{M}\mathbf{q}_m^2(n)\langle\tilde{\Phi}_k^{(\kappa)}(n), [G_{m,k}(n)]^2\rangle, \tag{57}
\end{aligned}
$$

where

$$
\begin{aligned}
\tilde{a}_k^{(\kappa)}(n) &\triangleq \rho_{k,n}(P^{(\kappa+1)}(n), q^{(\kappa)}(n)) - \langle\tilde{\Phi}_k^{(\kappa)}(n), \sigma^2 I_2\rangle \\
&\quad -\langle(\tilde{\Psi}^{(\kappa)}(n))^{-1}, [\mathcal{L}_{k,k}(q^{(\kappa)}(n))P_k^{(\kappa+1)}(n)]^2\rangle, \\
\tilde{B}_k^{(\kappa)}(n) &\triangleq (\tilde{\Psi}_k^{(\kappa)}(n))^{-1}\mathcal{L}_{k,k}(q^{(\kappa)}(n))[P_k^{(\kappa+1)}(n)]^2, \\
\tilde{\Psi}_k^{(\kappa)}(n) &\triangleq \sum_{j\neq k}^{K}[\mathcal{L}_{k,j}(q^{(\kappa)}(n))P_j^{(\kappa)}(n)]^2 \\
&\quad +\sigma_R^2\sum_{m=1}^{M}(q_m^{(\kappa)}(n))^2[G_{m,k}(n)]^2 + \sigma^2 I_2, \\
\tilde{\Phi}_k^{(\kappa)}(n) &\triangleq (\tilde{\Psi}^{(\kappa)}(n))^{-1} \\
&\quad -(\tilde{\Psi}^{(\kappa)}(n) + [\mathcal{L}_{k,k}(q^{(\kappa)}(n))P_k^{(\kappa+1)}(n)]^2)^{-1},
\end{aligned}
$$

It follows from that (39) that

$$\text{vec}(\mathcal{L}_{k,j}(\mathbf{q}(n))) = L_{k,j}(n)\mathbf{q}(n) \tag{58}$$

with $L_{k,j}(n) = \begin{bmatrix} \Re\{\ell_{k,j}^T(n)\} \\ \Im\{\ell_{k,j}^T(n)\} \\ -\Im\{\ell_{k,j}^T(n)\} \\ \Re\{\ell_{k,j}^T(n)\} \end{bmatrix} \in \mathbb{R}^{4 \times M}$. Then

$$
\begin{aligned}
\langle \tilde{B}^{(\kappa)}(n), \mathcal{L}_{k,k}(\mathbf{q}(n)) \rangle &= \langle \mathsf{vec}(\tilde{B}_k^{(\kappa)}(n)), \mathsf{vec}(\mathcal{L}_{k,k}(\mathbf{q}(n))) \rangle \\
&= \langle \mathsf{vec}(\tilde{B}_k^{(\kappa)}(n)), L_{k,k}(n)\mathbf{q}(n) \rangle \\
&= \langle L_{k,k}^T(n)\mathsf{vec}(\tilde{B}_k^{(\kappa)}(n)), \mathbf{q}(n) \rangle.
\end{aligned}
\tag{59}
$$

Furthermore,

$$
\begin{aligned}
& \langle \tilde{\Phi}_k^{(\kappa)}(n), [\mathcal{L}_{k,j}(\mathbf{q}(n)) P_j^{(\kappa+1)}(n)]^2 \rangle \\
&= \|\mathsf{vec}\left((\tilde{\Phi}_k^{(\kappa)}(n))^{1/2} \mathcal{L}_{k,j}(\mathbf{q}(n)) P_j^{(\kappa+1)}(n) \right)\|^2 \\
&= \|\left((P_j^{(\kappa+1)}(n))^T \otimes (\tilde{\Phi}_k^{(\kappa)}(n))^{1/2} \right) \mathsf{vec}\left(\mathcal{L}_{k,j}(\mathbf{q}(n)) \right)\|^2 \\
&= \|\left((P_j^{(\kappa+1)}(n))^T \otimes (\tilde{\Phi}_k^{(\kappa)}(n))^{1/2} \right) L_{k,j}(n)\mathbf{q}(n)\|^2 \\
&= (\mathbf{q}(n))^T \tilde{C}_{k,j}^{(\kappa)}(n)\mathbf{q}(n),
\end{aligned}
\tag{60}
$$

for

$$
\begin{aligned}
\tilde{C}_{k,j}^{(\kappa)}(n) &\triangleq L_{k,j}^T(n)\left(P_j^{(\kappa+1)}(n) \otimes (\tilde{\Phi}_k^{(\kappa)}(n))^{1/2} \right) \\
&\quad \times \left((P_j^{(\kappa+1)}(n))^T \otimes (\tilde{\Phi}_k^{(\kappa)}(n))^{1/2} \right) L_{k,j}(n) \\
&= L_{k,j}^T(n)\left([P_j^{(\kappa+1)}(n)]^2 \otimes \tilde{\Phi}_k^{(\kappa)}(n) \right) L_{k,j}(n).
\end{aligned}
\tag{61}
$$

Based on (56), (57), (58), (59), and (60), the following function $\tilde{F}^{(\kappa)}(\mathbf{q})$ turns out to be a tight concave quadratic minorant for the nonconcave function $F(P^{(\kappa+1)}, \mathbf{q})$:

$$
\begin{aligned}
& \tilde{F}^{(\kappa)}(\mathbf{q}) \\
&\triangleq \frac{1}{2} \sum_{k=1}^K \sum_{n=0}^{N-1} \tilde{\rho}_{k,n}^{(\kappa)}(\mathbf{q}(n)) \\
&= \frac{1}{2} \sum_{k=1}^K \sum_{n=0}^{N-1} \tilde{a}_k^{(\kappa)}(n) + 2 \sum_{n=0}^{N-1} \langle \tilde{\mathcal{L}}^{(\kappa)}(n), \mathbf{q}(n) \rangle \\
&\quad - \sum_{n=0}^{N-1} (\mathbf{q}(n))^T \tilde{D}^{(\kappa)}(n)\mathbf{q}(n),
\end{aligned}
\tag{62}
$$

for $\tilde{\mathcal{L}}^{(\kappa)}(n) \triangleq \sum_{k=1}^K L_{k,k}^T(n)\mathsf{vec}(\tilde{B}_k^{(\kappa)}(n))$, and $\tilde{D}^{(\kappa)}(n) \triangleq \sum_{k=1}^K \sum_{j=1}^K \tilde{C}_{k,j}^{(\kappa)}(n) + \sigma_R^2 \sum_{k=1}^K \mathsf{diag}[\langle \tilde{\Phi}_k^{(\kappa)}(n), [G_{m,k}(n)]^2 \rangle]_{m=1,\dots M}$.

We solve the following convex quadratic problem of minorant maximization to generate $q^{(\kappa+1)}$

$$
\max_{\mathbf{q}} \tilde{F}^{(\kappa)}(\mathbf{q}) \quad \text{s.t.} \quad (56).
\tag{63}
$$

This problem admits the closed-form solution

$$
q^{(\kappa+1)}(n) = \begin{cases} (\tilde{D}^{(\kappa)}(n))^{-1}\tilde{\mathcal{L}}^{(\kappa)}(n) & \text{if } \tilde{\Xi} \leq \tilde{P}_{tot}^{(\kappa)} \\ (\tilde{D}^{(\kappa)}(n) + \mu\tilde{\Theta}^{(\kappa)}(n))^{-1}\tilde{\mathcal{L}}^{(\kappa)}(n) & \text{otherwise,} \end{cases}
\tag{64}
$$

where $\tilde{\Xi} \triangleq \sum_{n=0}^{N-1} \|(\tilde{\Theta}^{(\kappa)}(n))^{1/2}(\tilde{D}^{(\kappa)}(n))^{-1}\tilde{\mathcal{L}}^{(\kappa)}(n)\|^2$ and $\mu > 0$ is found by bisection such that

---

Algorithm 2 Resource allocation algorithm for IGS based problem (47)

1: **Initialization**: Randomly generate $(P^{(0)}, q^{(0)},)$ satisfying the constraint (47b). Set $\kappa := 0$.
2: **Repeat until convergence of the objective function in** (47): Update $P^{(\kappa+1)}$ using (53) and then update $q^{(\kappa+1)}$ using (64). Reset $\kappa \leftarrow \kappa + 1$.
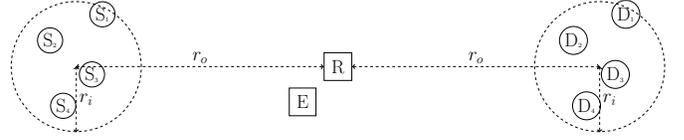

Fig. 2. An example network topology under $K = 4$ users.

$\sum_{n=0}^{N-1} \|(\tilde{\Theta}^{(\kappa)}(n))^{1/2}(\tilde{D}^{(\kappa)}(n) + \mu\tilde{\Theta}^{(\kappa)}(n))^{-1}\tilde{\mathcal{L}}^{(\kappa)}(n)\|^2 = \tilde{P}_{tot}^{(\kappa)}$.

Like (54), we can show that $(P^{(\kappa+1)}, q^{(\kappa+1)})$ is a better feasible point than $(P^{(\kappa+1)}, q^{(\kappa)})$, which together with (54) make $(P^{(\kappa+1)}, q^{(\kappa+1)})$ a better feasible point than $(P^{(\kappa)}, q^{(\kappa)})$. Algorithm 2 provides the pseudo-code for the alternating descent procedure based on the closed forms (53) and (64).

V. NUMERICAL RESULTS

In this section, we evaluate the performance of the proposed Algorithms 1 and 2. To model small scale fading, the SIMO channel between S_k and R, $\tilde{h}_k(\ell)$, and the MISO channel between R and D_k, $\tilde{g}_k(\ell)$, follow Rayleigh fading, where $\ell \in \{0, \dots, L-1\}$ is the index of the frequency-selective multipath channel. Our simulations consider an $L = 8$-tap multipath channel, which assumes a negative-exponentially decaying delay profile with the root-mean-square delay spread of T_s, for the symbol time $T_s = 1/B$ and the system bandwidth B Hz. On the other hand, the frequency-flat MIMO channel $\tilde{H}_E$, between E and R, follows Rician fading with Rician factor of 6 dB.

To model large scale fading, all S_k-to-R and R-to-D_k channel coefficients, $\tilde{h}_{k,m}(\ell)$ and $\tilde{g}_{m,k}(\ell)$, respectively, follow the path loss models of $30 + 10\beta \log_{10}(d_{S_k R})$ and $30 + 10\beta \log_{10}(d_{RD_k})$, respectively, where $\beta = 3$ is the path-loss exponent, while $d_{S_k R}$ and d_{RD_k} denote the S_k-to-R and R-to-D_k distance, respectively. As shown in Fig. 2, the source and destination nodes are randomly located in separate circular regions of $r_i = 20$ m radius, which are about $2r_o$ m apart. The relay is located mid-way between the two circular regions, at a distance of about r_o m from them. Unless stated otherwise, we set $r_o = 100$ m in our simulations. The large scale fading for the MIMO channel $\tilde{H}_E$, between E and R, follows the path loss model of $30 + 10\beta_E \log_{10}(d_{ER})$ with path loss exponent $\beta_E = 2$, while is $d_{ER} = 10$ m is the distance between E and R. The energy harvesting efficiency is set to $\eta = 0.5$. To ensure meaningful wireless power transfer to the energy harvesting node, typically smaller line-of-sight communication distance and hence smaller path-loss exponents are adopted in the literature [42].

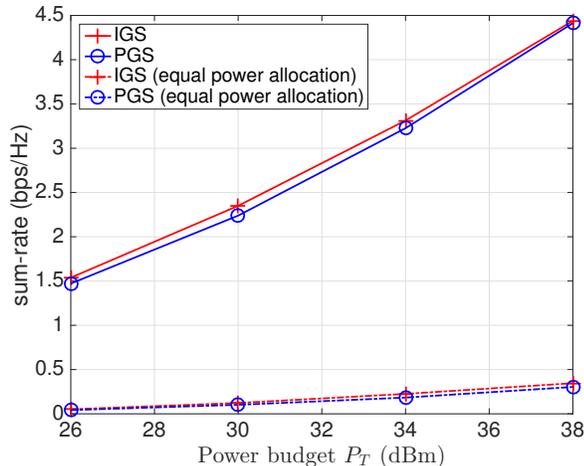The system bandwidth (BW) is set to $B = 5$ MHz and therefore the subcarrier BW is B/N. The noise power spectral

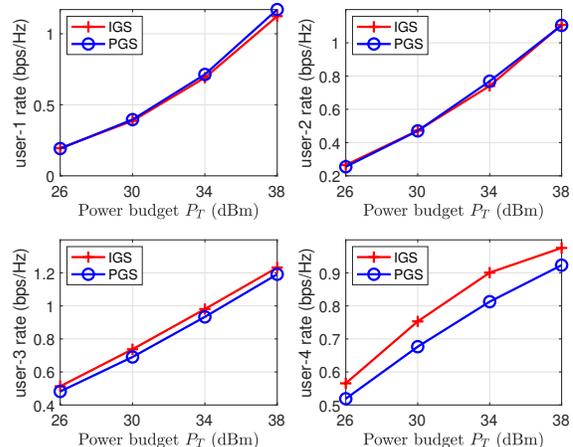Fig. 3. Average sum-rate versus the transmit power budget P_T.

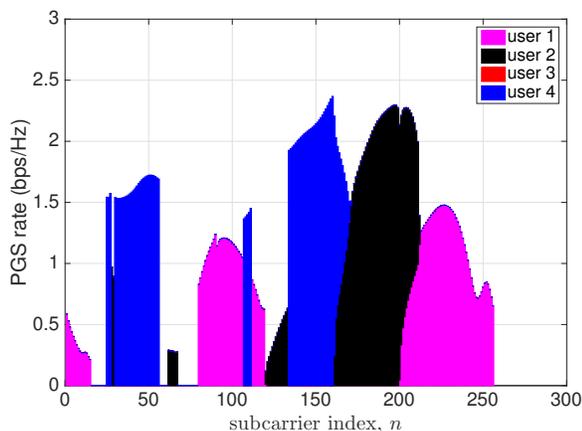Fig. 4. Average individual user-rate versus the transmit power budget P_T.

Fig. 5. The optimized user-rates for the proposed PGS based Alg. 1 versus the subcarrier index at $P_T = 30$ dBm.
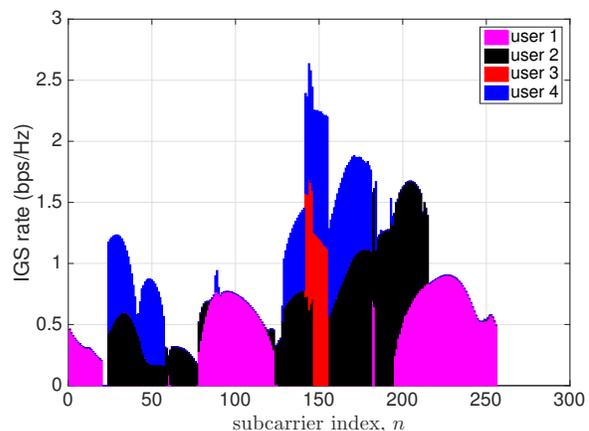

Fig. 6. The optimized user-rates for the proposed IGS based Alg. 2 versus the subcarrier index at $P_T = 30$ dBm.

density (noise per unit BW) over each subcarrier, i.e., $\frac{\sigma_R^2}{B/N}$ at each R's antenna and $\frac{\sigma^2}{B/N}$ at each D, is set to -174 dBm/Hz. The carrier frequency is set to 1 GHz. Unless specified otherwise, we set the total transmit power budget to $P_T = 30$ dBm, use $M = 4$ TAs and RAs at the relay, $N = 256$ subcarriers, $M_E = 4$ and $\gamma_{\text{LI}} = -10$ dB. The SI path gain of $\gamma_{\text{LI}} = -10$ dB is justified, since there is no source-to-relay information transfer during the second communication phase and there is no need to employ SI cancellation at the relay because the energy in the SI channel is recycled by the relay via wireless energy harvesting [12], [14]. We would like to mention here that under our simulation setup, the power received by the relay during its EH phase is in the range of $(50, 100)$ μW. In this range of received power, the harvested energy is linearly proportional to the input radio frequency (RF) power [43]–[45], which justifies our use of a simple linear EH model, especially because emphasis is on other challenges, not on the EH model.

Fig. 3 plots the average sum-rate versus the transmit power budget P_T for the proposed PGS and IGS based proposed Algorithms 1 and 2, respectively. The average sum-rate for the PGS-based Alg. 1 is calculated by evaluating $\frac{1}{N} \sum_{k=1}^{K} \sum_{n=0}^{N-1} r_{k,n}(\mathbf{p}, \mathbf{q})$ and averaging it over a large

number of simulations, where $r_{k,n}(\mathbf{p}, \mathbf{q})$ is given in (17) and the optimized values of $\mathbf{p}$ and $\mathbf{q}$ are obtained from Alg. 1. Similarly, the average sum-rate for the IGS-based Alg. 2 is calculated by evaluating $\frac{1}{2N} \sum_{k=1}^{K} \sum_{n=0}^{N-1} \rho_{k,n}(\mathbf{P}, \mathbf{q})$ and averaging it over a large number of simulations, where $\rho_{k,n}(\mathbf{P}, \mathbf{q})$ is given in (46) and optimized values of $\mathbf{P}$ and $\mathbf{q}$ are obtained from Alg. 2. Fig. 3 also plots the average sum-rate assuming equal power allocation, where we can observe the advantage of the proposed power allocation Algorithms 1 and 2 over equal-power allocation strategy. The performance gain increases upon increasing P_T. We can also observe the advantage of the IGS based Alg. 2 over the PGS based Alg. 1 in terms of its sum-rate performance. In order to check the rate of the individual user-pairs, Fig. 4 plots the average individual user-rate versus the transmit power budget P_T. We can also observe the advantage of the IGS based Alg. 2 over the PGS based Alg. 1 in terms of its individual user-rate performance, particularly for the communication of user-3 (S$_3$ $-$ D$_3$) and user-4 (S$_4$ $-$ D$_4$).

Figs. 5 and 6 plot the optimized user-rates for the proposed PGS based Alg. 1 and IGS based Alg. 2, respectively, over different subcarriers, for a certain fixed simulation. We can observe that some of the carriers are left unused, especially
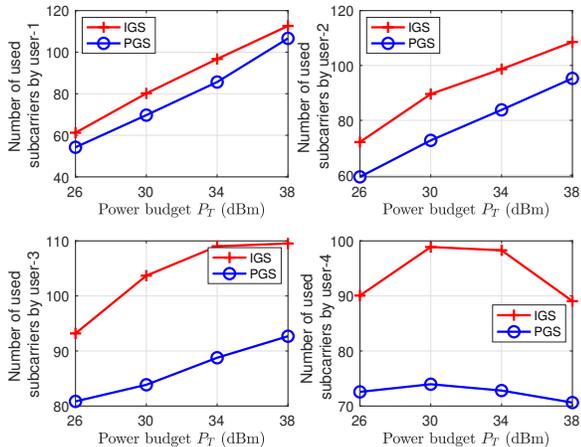
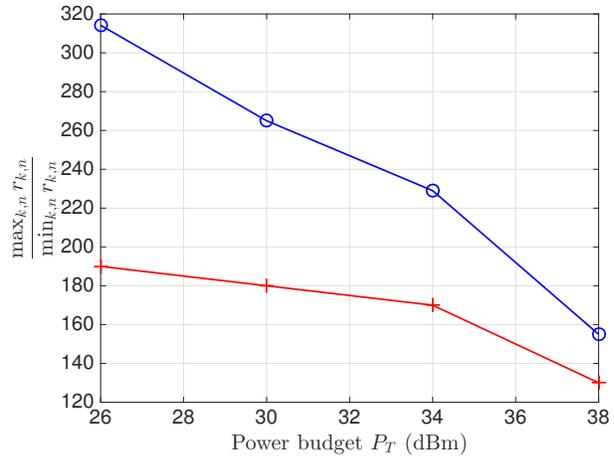Fig. 7. Average number of used subcarriers by all users versus the total power budget P_T.

Fig. 8. Average ratio of maximum subcarrier-rate to minimum subcarrier-rate (ignoring zero rate) versus the total power budget P_T.
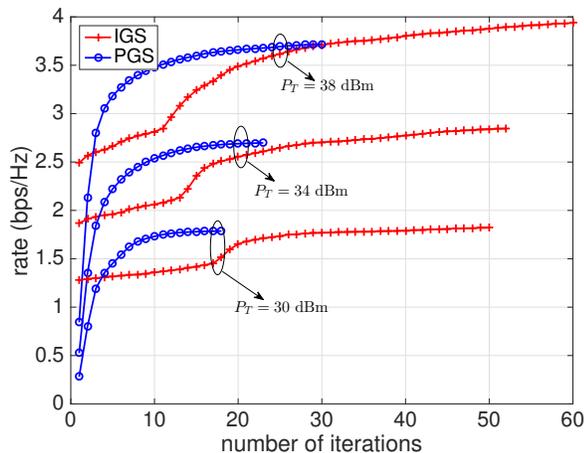

Fig. 9. The convergence of proposed Alg. 1 and Alg. 2

Fig. 10. Average sum-rate versus the transmit power budget P_T to show the advantage of self-energy recycling.

under PGS, which shows that the IGS promises a fairer distribution of the rates across different subcarriers. Particularly, we can observe from Fig. 5 that under PGS, user 3 fails to achieve an adequate rate over all the subcarriers. This emphasizes another benefit of IGS, namely its fairer rate distribution among the users, which is important for any real multi-user communication system.

Fig. 7 plots the average number of subcarriers assigned to the individual users. It can be observed from Fig. 7 that the IGS based Alg. 2 is more efficient than the PGS based Alg. 1, since it actively uses more subcarriers for the users.

Fig. 8 plots the average ratio of the maximum subcarrier-rate to minimum subcarrier-rate, where zero-rate subcarriers are ignored. Observe that the ratio of maximum subcarrier-rate to minimum subcarrier-rate is lower for the IGS based Alg. 2 than that for the PGS based Alg. 1, which shows that the IGS promises a more fair rate-distribution across the subcarriers.

Fig. 9 shows the convergence of the proposed Algorithms 1 and 2 for different values of the power budget P_T for a particular simulation. We can observe that the proposed PGS based Alg. 1 converges fairly promptly within 15-30 iterations, where both the required number of iterations and the optimized
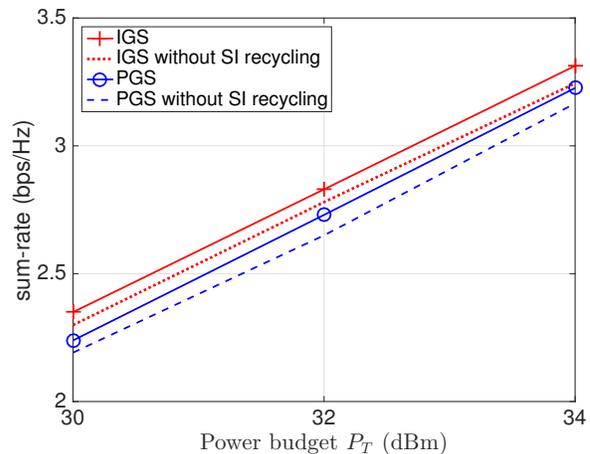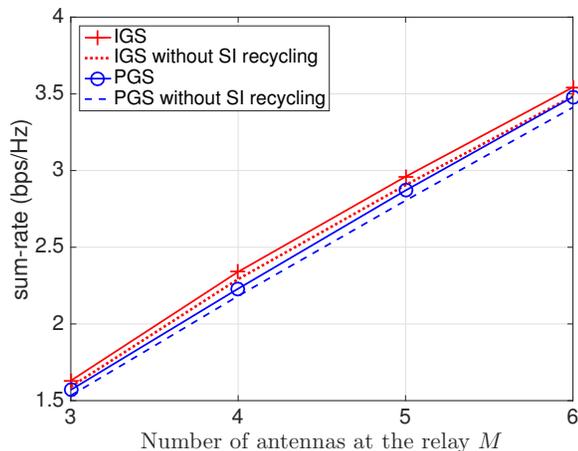
rate tend to increase upon increasing P_T. The same broad trend is observed for the proposed IGS based Alg. 2, but it requires more iterations (around 50-60) for convergence. This is because the IGS based Alg. 2 has to optimize $3KN$ higher number of optimization variables compared to the PGS based Alg. 1. It is noteworthy that the computational complexity of the proposed PGS and IGS based Algorithms 1 and 2 is $\mathcal{O}(N(K+M))$ and $\mathcal{O}(N(4K+M))$, respectively, which is very small, thanks to the proposed closed-form based solutions.

Fig. 10 plots the average sum-rate versus P_T to show the advantage of SI recycling. The phrase "without SI recycling" in the results implies that no SI recycling is carried out at the relay. In other words, the harvested energy due to SI recycling is ignored. These results can be obtained by assuming very low SI path gain, e.g., $\gamma_{\mathrm{LI}} = -100$ dB. We can observe that the improvement in the spectral efficiency due to SI recycling is around 0.045 bps/Hz at $P_T = 30$ dBm and the performance gain increases to 0.06 bps/Hz at $P_T = 34$ dBm. This implies a sum-rate improvement of around 0.225 Mbps at the system BW of 5 MHz, at $P_T = 30$ dBm.

Figs. 11 and 12 plot the average sum-rate and average
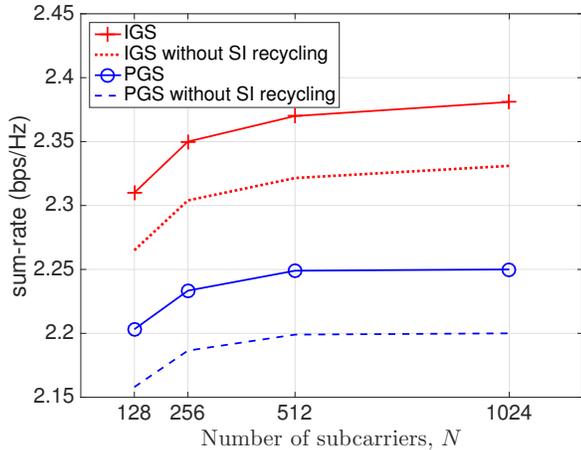
Fig. 11. Average sum-rate versus the total number of subcarriers N.

Fig. 12. Average individual user-rate versus the total number of subcarriers N.

Fig. 13. Average sum-rate versus number of antennas at the relay M.
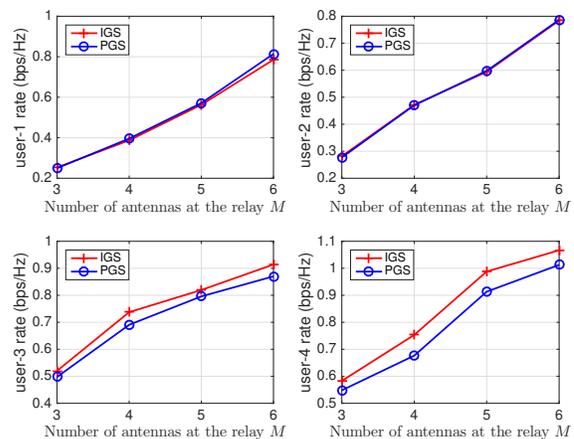
Fig. 14. Average individual user-rate versus number of antennas at the relay M.

individual user-rate, respectively, for the proposed PGS and IGS based Algorithms 1 and 2, respectively, versus the number of subcarriers N. We can observe that the spectral efficiency improves upon increasing the number of subcarriers. We can also observe the advantage of self-energy recycling and the dominance of IGS based Alg. 2 over PGS based Alg. 1 in terms of both the sum-rate and individual user-rate.

Figs. 13 and 14 plot the average sum-rate and average individual user-rate, respectively, for the proposed PGS and IGS based Algorithms 1 and 2, respectively, versus number of antennas M at the relay. The spectral efficiency improves upon increasing M due to the increase in the spatial diversity order at the relay. Still referring to Figs. 13 and 14, we can also observe the advantage of self-energy recycling and the dominance of IGS based Alg. 2 over PGS based Alg. 1 in terms of both its sum-rate and individual user-rate versus M.

Fig. 15 plots the average sum-rate for the proposed PGS and IGS based Algorithms 1 and 2, respectively, versus the SI path gain γ_{LI}. Fig. 15 also plots the sum-rate of a system that does not employ SI recycling. Observe that in contrast to the non-EH based systems, where the SI degrades the simultaneous signal transmission and reception, the SI in Fig. 15 enhances the sum-rate. For example, it can be seen from
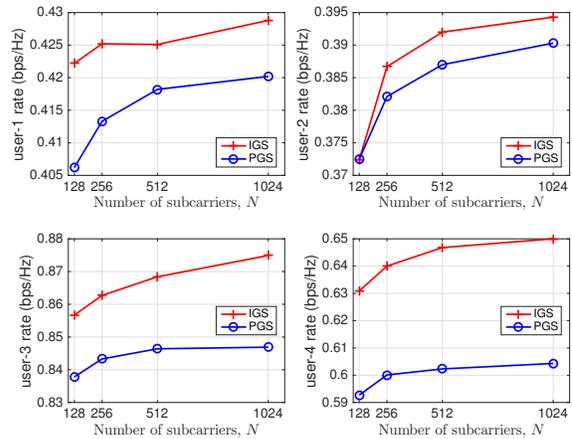
Fig. 15 that the spectral efficiency improvement of the IGS based system due to SI recycling is in the range of $(0.02, 0.38)$ bps/Hz for the values of $\gamma_{\mathrm{LI}} = (-14, -2)$ dB, which implies the sum-rate improvement in the range of $\{0.1, 1.9\}$ Mbps at the system BW of 5 MHz. The spectral efficiency improves upon increasing the SI path gain due to the SI attenuation reduction at the relay. Furthermore, we note that the advantage of SI recycling manifests itself not only in terms of improving the achievable data rate, the wireless power exploited via SI recycling also assists the energy-constrained relay node in replenishing its battery.

Fig. 16 plots the average sum-rate for the proposed PGS and IGS based Algorithms 1 and 2, respectively, versus the separation between the relay and users locality r_o (which is defined in Fig. 2). The spectral efficiency is reduced upon increasing r_o due to the increase in path-loss. We can also observe the dominance of the IGS based Alg. 2 over the PGS based Alg. 1 and the advantage of SI recycling.

Fig. 17 plots the average ratio of the maximum subcarrier-rate to minimum subcarrier-rate, where the zero-rate subcarriers are ignored. Observe that the ratio of maximum subcarrier-rate to minimum subcarrier-rate is lower for the IGS based Alg. 2 than that for the PGS based Alg. 1, which shows that the
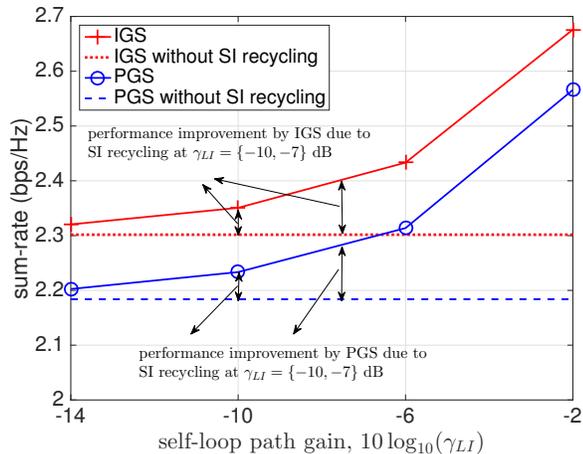
Fig. 15. Average sum-rate versus SI path gain γ_{LI}.

Fig. 16. Average sum-rate versus separation between relay and users locality r_o (r_o is defined in Fig. 2).
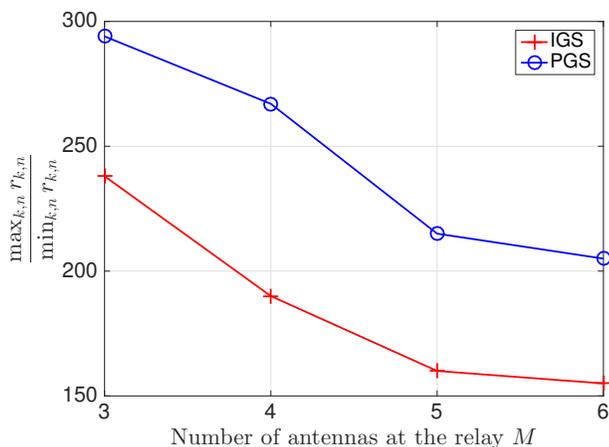

Fig. 17. Average ratio of maximum subcarrier-rate to minimum subcarrier-rate (ignoring zero rate) versus number of antennas at the relay M.

IGS promises a fairer-rate distribution across the subcarriers.

VI. Conclusions

Simultaneous energy harvesting and recycling was proposed for relay-aided multi-user OFDM systems, where the source and destination nodes are located far from each other, hence requiring a relay's assistance. Both proper and improper Gaussian signaling have been considered at the source. The challenging sum-throughput maximization problems of the joint power allocation design of multiple sources and a common relay node are solved. Particularly, alternating descent algorithms were developed, which are based on closed-form expressions at each iteration, and thus are quite practical, regardless of the scale of the non-convex problems considered. The pros and cons of PGS vs. IGS were discussed, where the latter has been shown to have a more fairer rate distribution across the subcarriers. The improvement in the sum-rate due to the recycled SI is shown to be about 0.045 bps/Hz over a wide-range of considered simulation parameters. The extension of the treatise to OFDM relaying for multi-user ultra relia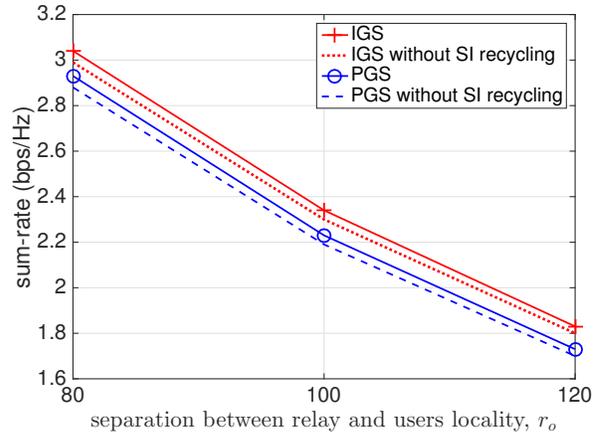ble and low-latency communication (MU-URLLC) is under our current study. Another possible future extension is to consider multiple antennas at both the source and destination nodes.

References

[1] D. N. K. Jayakody, J. Thompson, S. Chatzinotas, and S. Durrani, Eds., *Wireless Information and Power Transfer: A New Paradigm for Green Communications*. Springer International Publishing, 2018.

[2] J. Hu, K. Yang, G. Wen, and L. Hanzo, "Integrated data and energy communication network: A comprehensive survey," *IEEE Commun. Surveys Tuts.*, vol. 20, no. 4, pp. 3169–3219, Fourthquarter 2018.

[3] X. Lu, P. Wang, D. Niyato, D. I. Kim, and Z. Han, "Wireless networks with RF energy harvesting: A contemporary survey," *IEEE Commun. Surveys Tuts.*, vol. 17, pp. 757–789, 2015.

[4] A. A. Nasir, H. D. Tuan, D. T. Ngo, T. Q. Duong, and H. V. Poor, "Beamforming design for wireless information and power transfer systems: Receive power-splitting vs transmit time-switching," *IEEE Trans. Commun.*, vol. 65, no. 2, pp. 876–889, 2017.

[5] A. A. Nasir, H. D. Tuan, T. Q. Duong, and H. V. Poor, "Secure and energy-efficient beamforming for simultaneous information and energy transfer," *IEEE Trans. Wirel. Commun.*, vol. 16, no. 11, pp. 7523–7537, Nov 2017.

[6] A. A. Nasir, H. D. Tuan, T. Q. Duong, and L. Hanzo, "Transmitter-side time-switching for wireless information and energy transfer in massive MIMO systems," *IEEE Trans. Vehic. Techn.*, vol. 69, no. 2, pp. 2322–2326, Feb. 2020.

[7] Z. Zhang, X. Chai, K. Long, A. V. Vasilakos, and L. Hanzo, "Full duplex techniques for 5G networks: self-interference cancellation, protocol design, and relay selection," *IEEE Commun. Mag.*, vol. 53, no. 5, pp. 128–137, May 2015.

[8] B. K. Chalise, H. A. Suraweera, G. Zheng, and G. K. Karagiannidis, "Beamforming optimization for full-duplex wireless-powered MIMO systems," *IEEE Trans. Commun.*, vol. 65, no. 9, pp. 3750–3764, Sep. 2017.

[9] Z. Sheng, H. D. Tuan, T. Q. Duong, H. V. Poor, and Y. Fang, "Low-latency multiuser two-way wireless relaying for spectral and energy efficiencies," *IEEE Trans. Signal Process.*, vol. 66, no. 16, pp. 4362–4376, Aug. 2018.

[10] A. A. Nasir, H. D. Tuan, and T. Q. Duong, "Fractional time exploitation for serving IoT users with guaranteed QoS by 5G spectrum," *IEEE Commun. Mag.*, vol. 56, no. 10, pp. 128–133, Oct. 2018.

[11] H. Yu, H. D. Tuan, T. Q. Duong, H. V. Poor, and Y. Fang, "Optimization for simultaneous signal transmission and reception in macrocell of heterogeneous uplinks and downlinks," *IEEE Trans. Commun.*, vol. 68, no. 11, pp. 7054–7067, Nov. 2020.

[12] Y. Zeng and R. Zhang, "Full-duplex wireless-powered relay with self-energy recycling," *IEEE Wirel. Commun. Letts.*, vol. 4, no. 2, pp. 201–204, Apr. 2015.

[13] A. A. Nasir, H. D. Tuan, T. Q. Duong, and H. V. Poor, "MIMO-OFDM-based wireless-powered relaying communication with an energy recycling interface," *IEEE Trans. Commun.*, vol. 68, no. 2, pp. 811–824, Feb. 2020.

[14] L. Zhang, Y. Cai, M. Zhao, B. Champagne, and L. Hanzo, "Nonlinear MIMO transceivers improve wireless-powered and self-interference-aided relaying," *IEEE Trans. Wirel. Commun.*, vol. 16, no. 10, pp. 6953–6966, Oct 2017.

[15] Z. Wei, X. Zhu, S. Sun, Y. Jiang, A. Al-Tahmeesschi, and M. Yue, "Research issues, challenges, and opportunities of wireless power transfer-aided full-duplex relay systems," *IEEE Access*, vol. 6, pp. 8870–8881, 2018.

[16] D. Hwang, S. S. Nam, and J. Yang, "Multi-antenna beamforming techniques in full-duplex and self-energy recycling systems: Opportunities and challenges," *IEEE Commun. Mag.*, vol. 55, no. 10, pp. 160–167, Oct. 2017.

[17] Z. Chu, F. Zhou, P. Xiao, Z. Zhu, D. Mi, N. Al-Dhahir, and R. Tafazolli, "Resource allocation for secure wireless powered integrated multicast and unicast services with full duplex self-energy recycling," *IEEE Trans. Wirel. Commun.*, vol. 18, no. 1, pp. 620–636, 2019.

[18] J. Qiao, H. Zhang, F. Zhao, and D. Yuan, "Secure transmission and self-energy recycling with partial eavesdropper CSI," *IEEE J. Sel. Areas Commun.*, vol. 36, no. 7, pp. 1531–1543, 2018.

[19] M. H. N. Shaikh, V. A. Bohara, and A. Srivastava, "Performance analysis of a full-duplex MIMO decode-and-forward relay system with self-energy recycling," *IEEE Access*, vol. 8, pp. 226 248–226 266, 2020.

[20] R. Kumar and A. Hossain, "Full-duplex wireless information and power transfer in two-way relaying networks with self-energy recycling," *Wireless Networks*, vol. 26, no. 8, p. 6139–6154, 2020.

[21] K. Kwon, D. Hwang, and S. S. Nam, "Beamformer design for self-energy recycling in full-duplex decode-and-forward relay systems," *IEEE Wirel. Commun. Lett.*, vol. 9, no. 9, pp. 1417–1421, 2020.

[22] W. Wu, B. Wang, Y. Zeng, H. Zhang, Z. Yang, and Z. Deng, "Robust secure beamforming for wireless powered full-duplex systems with self-energy recycling," *IEEE Trans. Veh. Technol.*, vol. 66, no. 11, pp. 10 055–10 069, Nov. 2017.

[23] M. Mohammadi, B. K. Chalise, H. A. Suraweera, C. Zhong, G. Zheng, and I. Krikidis, "Throughput analysis and optimization of wireless-powered multiple antenna full-duplex relay systems," *IEEE Trans. Commun.*, vol. 64, no. 4, pp. 1769–1785, April 2016.

[24] A. Yadav, O. A. Dobre, and H. V. Poor, "Is self-interference in full-duplex communication: a foe or a friend?" *IEEE Signal Process. Letts.*, vol. 25, no. 7, pp. 951–955, July 2018.

[25] H. Liu, K. J. Kim, K. S. Kwak, and H. V. Poor, "Power splitting-based SWIPT with decode-and-forward full-duplex relaying," *IEEE Trans. Wirel. Commun.*, vol. 15, no. 11, pp. 7561–7577, Nov 2016.

[26] Q. N. Le, V. N. Q. Bao, and B. An, "Full-duplex distributed switch-and-stay energy harvesting selection relaying networks with imperfect CSI: Design and outage analysis," *J. Commun. Networks*, vol. 20, no. 1, pp. 29–46, Feb 2018.

[27] O. T. Demir and T. E. Tuncer, "Robust optimum and near-optimum beamformers for decode-and-forward full-duplex multi-antenna relay with self-energy recycling," *IEEE Trans. Wirel. Commun.*, vol. 18, no. 3, pp. 1566–1580, 2019.

[28] A. Goldsmith, *Wireless Commununications*. New York, NY, USA: Cambridge University Press, 2005.

[29] T. M. Hoang, A. E. Shafie, D. B. da Costa, T. Q. Duong, H. D. Tuan, and A. Marshall, "Security and energy harvesting for MIMO-OFDM networks," *IEEE Trans. Commun.*, vol. 68, no. 4, pp. 2593–2606, Apr. 2020.

[30] P. J. Schreier and L. L. Scharf, *Statistical signal processing of complex-valued data: The theory of improper and noncircular signals*. Cambridge University Press, 2010.

[31] C. Lameiro, I. Santamaría, and P. J. Schreier, "Rate region boundary of the SISO Z-interference channel with improper signaling," *IEEE Trans. on Commun.*, vol. 65, no. 3, pp. 1022–1034, March 2017.

[32] S. Lagen, A. Agustin, and J. Vidal, "Coexisting linear and widely linear transceivers in the MIMO interference channel," *IEEE Trans. Signal Process.*, vol. 64, no. 3, pp. 652–664, Feb 2016.

[33] H. D. Tuan, A. A. Nasir, H. H. Nguyen, T. Q. Duong, and H. V. Poor, "Non-orthogonal multiple access with improper Gaussian signaling," *IEEE J. Sel. Areas Signal Process.*, vol. 13, no. 3, pp. 496–507, Jun. 2019.

[34] A. A. Nasir, H. D. Tuan, H. H. Nguyen, T. Q. Duong, and H. V. Poor, "Signal superposition in NOMA with proper and improper Gaussian signaling," *IEEE Trans. Commun.*, vol. 68, no. 10, pp. 6537–6551, Oct. 2020.

[35] H. Yu, H. D. Tuan, T. Q. Duong, Y. Fang, and L. Hanzo, "Improper Gaussian signaling for integrated data and energy networking," *IEEE Trans. Commun.*, vol. 68, no. 6, pp. 3922–3934, Jun. 2020.

[36] H. Yu, H. D. Tuan, A. A. Nasir, T. Q. Duong, and H. V. Poor, "Joint design of reconfigurable intelligent surface and transmit beamforming under proper and improper Gaussian signaling," *IEEE J. Selec. Areas Commun.*, vol. 38, no. 11, pp. 2589–2603, Nov. 2020.

[37] M. Soleymani, C. Lameiro, P. J. Schreier, and I. Santamaria, "Improper signaling for OFDM underlay cognitive radio systems," in *Proc. 2018 IEEE Stat. Signal Process. Work. (SSP)*, 2018, pp. 722–726.

[38] R. A. Horn and C. R. Johnson, *Matrix analysis*. Cambridge University Press, 1985.

[39] H. H. M. Tam, H. D. Tuan, and D. T. Ngo, "Successive convex quadratic programming for quality-of-service management in full-duplex MU-MIMO multicell networks," *IEEE Trans. Commun.*, vol. 64, pp. 2340–2353, Jun. 2016.

[40] H. Tuy, *Convex Analysis and Global Optimization (second edition)*. Springer International, 2017.

[41] T. M. Cover and J. A. Thomas, *Elements of Information Theory (second edition)*. John Wileys & Sons, 2006.

[42] A. Ghazanfari, H. Tabassum, and E. Hossain, "Ambient RF energy harvesting in ultra-dense small cell networks: performance and trade-offs," *IEEE Wirel. Commun.*, vol. 23, no. 2, pp. 38–45, April 2016.

[43] E. Boshkovska, D. W. K. Ng, N. Zlatanov, and R. Schober, "Practical non-linear energy harvesting model and resource allocation for SWIPT systems," *IEEE Commun. Lett.*, vol. 19, no. 12, pp. 2082–2085, 2015.

[44] T. Le, K. Mayaram, and T. Fiez, "Efficient far-field radio frequency energy harvesting for passively powered sensor networks," *IEEE J. Solid-State Circuits*, vol. 43, no. 5, pp. 1287–1302, 2008.

[45] J. Guo and X. Zhu, "An improved analytical model for RF-DC conversion efficiency in microwave rectifiers," in *Proc. IEEE MTT-S MTT-S Int. Microw. Symp.*, 2012, pp. 1–3.